RSC Advances

ROYAL SOCIETY OF CHEMISTRY

PAPER

View Article Online
View Journal | View Issue

Cite this: *RSC Adv.*, 2026, **16**, 5013

Eco-engineered bio-based palladium MOF–chitosan–carboxymethyl cellulose composite sponge: mechanistic insights, Box–Behnken optimization, and high-performance reusability for advanced ciprofloxacin removal from wastewater

Naoufel Ben Hamadi,[a] Ahlem Guesmi,[a] Wesam Abd El-Fattah,[a] Basmah H. Alshammari,[b] Naflaa A. Aldawsari,[c] Mohamed G. El-Desouky[d] and Ashraf A. El-Bindary *[e]

In this work,a new bio-based palladium metal–organic framework (Pd-MOF)/chitosan (CS)–carboxymethyl cellulose (CMC) composite (PMCC) sponge created by inserting a Pd-MOF into a medium comprising CS and CMC. The PMCC sponge was produced *via* a straightforward, environmentally friendly technique and was verified as an effective adsorbent for removing ciprofloxacin (CIP), a commonly used fluoroquinolone antibiotic, from water. A thorough classification of the sponge was conducted using methods such as FTIR spectroscopy, XPS, XRD, BET analysis, and SEM-EDX mapping. These methods confirmed the successful integration and porous nature of the composite material. Moreover, batch adsorption experiments were performed to evaluate how factors such as pH, contact time, adsorbent quantity, and temperature affected the uptake of CIP. The adsorption process adhered to the Langmuir isotherm model, with an adsorption energy of 33.6 kJ mol^{-1}, suggesting that the mechanism is chemisorption. The kinetic behavior was predominantly characterized by the pseudo-second-order model. A thermodynamic evaluation specified that the adsorption was both spontaneous and endothermic, with an enthalpy ($\Delta H°$) of 91.2 kJ mol^{-1} and entropy ($\Delta S°$) of 315.2 J mol^{-1} K^{-1}. The proposed adsorption mechanism involves interactions such as hydrogen bonding, $\pi-\pi$ interactions, and electrostatic forces. Furthermore, the PMCC demonstrated excellent reusability, retaining substantial adsorption capacity after five regeneration cycles. An optimization process utilizing the Box–Behnken design established the adsorbent's competency under ideal conditions. Overall, these results position the PMCC sponge as a practical, reusable, and eco-friendly solution for the elimination of antibiotics from polluted water sources.

Received 1st November 2025
Accepted 14th December 2025

DOI: 10.1039/d5ra08409a

rsc.li/rsc-advances

1. Introduction

Fluoroquinolones represent a widely used category of antibiotics, which includes drugs like ciprofloxacin, norfloxacin, and levofloxacin. The extensive use of these medications, combined with their inadequate elimination through conventional wastewater-treatment processes, has resulted in their frequent presence in aquatic environments. These antibiotics are characterized by their durability, structural integrity, and resistance to biodegradation, enabling them to persist in water systems and pose significant environmental risks.[1] Fluoroquinolones can negatively impact the growth and metabolic processes of aquatic microorganisms, accumulate within fish and invertebrates, and interfere with the reproductive and developmental functions of various aquatic species. Notably, even at low concentrations, they can place selective pressure on structured microbial societies, contributing to the dissemination of antibiotic resistance genes. These genes are capable of being transferred to pathogenic bacteria, potentially compromising the effectiveness of vital antibiotics used as human medicines.[2] Furthermore, the presence of fluoroquinolones in wastewater can impair the efficiency of biological treatment systems and result in the contamination of downstream drinking water sources, raising serious long-term health and environmental

[a]*Chemistry Department, College of Science, Imam Mohammad Ibn Saud Islamic University (IMSIU), P.O. Box 5701, Riyadh 11432, Saudi Arabia*
[b]*Chemistry Department, College of Science, University of Hail, Ha'il 81451, Saudi Arabia*
[c]*Chemistry Department, Al-Khurrmah University College, Taif University, Al-Khurrmah 21985, Saudi Arabia*
[d]*Egyptian Propylene and Polypropylene Company, Port Said 42511, Egypt*
[e]*Chemistry Department, Faculty of Science, Damietta University, Damietta 34517, Egypt. E-mail: abindary@du.edu.eg*

issues. Therefore, it is essential to adopt effective strategies for the elimination of fluoroquinolones from wastewater to safeguard water ecosystems, mitigate public health risks, and foster sustainable water-management practices.[3]

One important class of synthetic antibiotics widely used in both human and veterinary medicines is fluoroquinolones. Notable examples include ciprofloxacin, norfloxacin, ofloxacin, levofloxacin, and moxifloxacin. The presence of a fluorine atom at the quinolone structure's C-6 position, which adds to the antibiotics' broad-spectrum antibacterial activity, makes them distinguishable. Among these, ciprofloxacin is frequently prescribed and often found in municipal, hospital, and industrial wastewater. Its highwater solubility, along with partial metabolic breakdown and resistance to biodegradation, means that a considerable amount of administered ciprofloxacin is excreted in its active form, entering aquatic systems through sewage discharge. The detection of ciprofloxacin in water bodies raises significant ecological concerns, as it can accumulate in aquatic life, interfere with photosynthesis in algae, and disrupt the microbial balance within sediment and biofilm communities.[4] Furthermore, ciprofloxacin exerts a potent selective pressure that promotes the development and dissemination of bacteria and genes resistant to antibiotics, thereby presenting an ongoing risk to public health worldwide. Additionally, it can negatively affect the performance of biological action systems by diminishing vital microbial activity, thereby reducing the overall treatment efficiency. Consequently, the effective elimination of ciprofloxacin from wastewater is crucial to mitigating its ecotoxicological effects, managing the spread of antimicrobial resistance, safeguarding biodiversity, and securing drinking water supplies, making it an essential target for the development of advanced, sustainable water purification technologies.[5]

Ciprofloxacin is a commonly utilized fluoroquinolone antibiotic that has become a focal point for removal from wastewater through various treatment technologies. These include advanced oxidation procedures (AOPs), membrane filtration, organic degradation, electrochemical approaches, and adsorption. AOPs, such as UV/H_2O_2, ozonation, and Fenton reactions, utilize reactive oxygen species for the degradation of ciprofloxacin; however, they are often hindered by high energy consumption, incomplete mineralization, and the formation of toxic byproducts. Membrane techniques, like nanofiltration and reverse osmosis, exhibit high removal efficiency, yet they face challenges such as membrane fouling, elevated costs, and difficulty in the management of concentrated waste streams. Biological treatment methods, which employ activated sludge or specific microbial strains, demonstrate limited effectiveness due to ciprofloxacin's resistance to biodegradation and its negative impact on microbial communities.[6] Electrochemical techniques can degrade ciprofloxacin but require expensive equipment and consume significant energy. Alternatively, adsorption has emerged as a particularly advantageous method because of its operational ease, cost-effectiveness, and environmental friendliness. This technique is capable of effectively removing ciprofloxacin even at low concentrations through forces, such as hydrogen bonding, electrostatic attraction, and π–π interactions, all without generating harmful secondary pollutants. Additionally, adsorption can utilize renewable or waste-derived adsorbents, like activated carbon, biochar, chitosan, and MOFs, which support sustainability. The adsorption process is easily scalable, can be integrated with other treatment methods, and facilitates the regeneration and reusability of adsorbents across multiple cycles, positioning it as an efficient, environmentally sound, and economically feasible solution for treating antibiotic-contaminated wastewater.[7]

Metal–organic frameworks (MOFs) are an innovative category of porous materials that provide notable benefits for the adsorption, as well as elimination of ciprofloxacin, in wastewater, attributed to their distinct structural and chemical characteristics.[8] Metal ions or clusters connected to organic ligands generate these crystalline structures, which produce well-defined three-dimensional frameworks with incredibly large surface areas, tunable pore diameters, and a diverse range of functional groups.[9] The large surface area provides many active sites for the adsorption of ciprofloxacin molecules, and the adjustable pore sizes enable selective absorption according to the molecular size and structure of the antibiotic. Furthermore, the MOF structure's functional groups facilitate a number of interaction processes, including π–π stacking, hydrogen bonding, electrostatic forces, and metal–ligand coordination with ciprofloxacin's amine, carboxyl, and aromatic rings. MOFs can be chemically altered or modified after synthesis to boost their selective affinity for particular pollutants.[10] Notably, numerous MOFs demonstrate robust chemical and thermal stability, and they can be integrated into biopolymer matrices, like chitosan or carboxymethyl cellulose, to enhance their water solubility, mechanical durability, and recyclability. These hybrid materials address practical challenges associated with MOF powders, such as particle aggregation and leaching, while retaining effective adsorption capabilities. Moreover, MOFs are typically regenerable, permitting multiple adsorption and desorption cycles with minimal performance degradation. Their compatibility with environmentally friendly synthesis techniques and capability to function under mild conditions position them as a sustainable and effective solution for the effective removal of ciprofloxacin from polluted water bodies.[10]

The integration of MOFs within biopolymeric matrices, specifically chitosan and carboxymethyl cellulose, presents an effective route to improve their efficacy, practicality, and environmental sustainability in the adsorption, as well as removal, of ciprofloxacin from pollutants. Although MOFs inherently possess high surface areas, adjustable porosity, and various functional sites that facilitate strong interactions with ciprofloxacin, they face challenges, such as limited water stability, difficulties in handling fine powders, and risks of secondary contamination through particle leaching. By encapsulating MOFs in CS and CMC, these challenges can be addressed.[11] Chitosan, a naturally derived polymer abundant in amino and hydroxyl groups, contributes additional active sites that promote hydrogen bonding and electrostatic interactions with ciprofloxacin. Simultaneously, CMC improves water dispersibility, structural integrity, and hydrophilicity because of

its carboxylate groups. The synergy between these biopolymers and MOFs results in a durable, flexible, and highly porous composite sponge with an enhanced adsorption capacity. This composite not only increases mechanical strength and reusability but also enhances resistance to degradation in aqueous environments. Furthermore, the composite format facilitates easier recovery and regeneration of the adsorbent, thereby reducing operational costs and minimizing environmental impact. This bio-based hybrid approach embodies the principles of green chemistry by leveraging renewable and biodegradable materials along with mild synthesis conditions, presenting a sustainable and actual method for eliminating persistent antibiotics, like ciprofloxacin, from pharmaceutical and municipal wastewater.[11]

The Box–Behnken design (BBD) is an effective statistical process utilized in response surface methodology (RSM), particularly advantageous for optimizing adsorption processes, such as the removal of ciprofloxacin from wastewater. A key advantage of BBD lies in its capacity to evaluate the interaction effects among various independent variables (pH, adsorbent amount, temperature, and interaction time) on adsorption performance, with a reduced number of investigational runs, thereby minimizing time, cost, and resource usage. In contrast to occupied factorial designs, BBD forgoes extreme variable combinations that may be impractical or hazardous, which enhances the reliability of the experiments.[12] Furthermore, BBD enables the formulation of precise prediction models through second-order polynomial equations that encompass both linear and nonlinear variable effects, facilitating the accurate determination of optimal conditions for maximizing adsorption capacity. The design also allows for the progress of three-dimensional surface plans and contour maps that visualize the interactions and relationships among variables, aiding in the comprehension of their impact on the response. Additionally, the statistical meaning and sufficiency of the model can be evaluated through ANOVA, ensuring the strength of the optimization outcomes. When applied to ciprofloxacin adsorption, the Box–Behnken design not only simplifies the optimization process but also deepens the scientific insight into how different operational parameters interact, ultimately supporting the advancement of more effective, reproducible, and scalable water-treatment solutions.[13]

This manuscript introduces a novel bio-based composite sponge for the effective adsorption and elimination of ciprofloxacin from water. The sponge is made with Pd-MOF embedded in the CS–CMC matrix. The Pd-MOF provides a high surface area with adjustable active sites, while chitosan's amine-rich groups enhance adsorption through hydrogen bonding and electrostatic interactions. CMC adds hydrophilicity, structural integrity, and carboxylate functionalities for effective adsorption. Unlike traditional MOF powders, the PMCC sponge offers a strong, porous structure that enhances practicality, strength, and reusability for wastewater treatment. Comprehensive characterization methods, including XRD, FTIR spectroscopy, BET analysis, SEM-EDX, and XPS, validate the structural integrity and adsorption mechanisms. Kinetic and thermodynamic modeling studies reveal that the adsorption procedure is spontaneous and influenced mainly by chemisorption. With fewer experiments, the Box–Behnken design optimizes the procedure with statistically verified improvements. This research presents a sustainable and cost-effective composite adsorbent for treating wastewater contaminated by pharmaceuticals.

2. Experimental

2.1. Materials and tools

As shown in Tables S1 and S2, the additional materials offer an inclusive summary of the materials and tools used.

2.2. Synthesis of the adsorbent

2.2.1. Synthesis of Pd-MOF. The Pd-MOF was synthesized utilizing a solvothermal approach, with palladium(II) nitrate dihydrate serving as the metal precursor and 1,3,5-benzenetricarboxylic acid (H_3BTC) functioning as the organic linker. In the initial step, 0.133 g of $Pd(NO_3)_2 \cdot 2H_2O$ was liquified in a 10-mL solvent mixture of DMF and distilled water, employing a 1 : 1 volume ratio while maintaining continuous magnetic stirring. Concurrently, 0.105 g of H_3BTC was dissolved in 10 mL of the identical solvent system.[14] The ligand solution was incrementally introduced dropwise to the metal solution, with continuous stirring implemented to facilitate uniform mixing and pre-coordination processes. This mixture underwent an additional stirring phase for 60 min at ambient temperature. Subsequently, it was moved into a Teflon-lined autoclave made of stainless-steel. Following the sealing of the autoclave, it was exposed to heat treatment at 140 °C for a period of 24 hours, thereby enhancing the formation of Pd-MOF crystals *via* the coordination interactions among Pd(II) ions and the carboxyl groups present in H_3BTC. After the autoclave process was finished, the mixture was permitted to cool down to room temperature through natural means. The resulting solid product was then retrieved *via* centrifugation. The Pd-MOF underwent multiple washing cycles with both ethanol and distilled water to eliminate any unreacted resources and leftover solvents. Subsequently, the product was dehydrated in an oven at 65 °C for 15 hours. The final Pd-MOF demonstrated a highly porous crystalline architecture, indicating its potential effectiveness for adsorption-related applications.

2.2.2. Encapsulating Pd-MOF with chitosan and carboxymethyl cellulose, crosslinked using itaconic acid (PMCC sponge). The synthesized Pd-MOF was integrated into a biopolymeric matrix that consisted of chitosan (CS) and carboxymethyl cellulose (CMC), utilizing itaconic acid as an environmentally friendly, bifunctional crosslinking agent. In order to create a transparent solution, chitosan (0.5 g) was first dissolved in 50 mL of acetic acid solution (1% (v/v)) with continuous stirring. Simultaneously, 0.5 g of CMC was dispersed in 50 mL of distilled water and stirred separately.[15] These two solutions were then mixed and stirred carefully to achieve a homogeneous mixture of CS and CMC. Following this, a predetermined amount of the synthesized Pd-MOF (for instance, 0.2 g) was introduced into the polymeric blend, and

a brief sonication process was performed to ensure the even distribution of the MOF particles throughout the matrix. A 1% (w/v) solution of itaconic acid was added gradually to the mixture, serving as a crosslinker that promotes esterification and hydrogen bonding among the hydroxyl and amine groups of the biopolymers and the carboxylic groups of itaconic acid. The mixture was continuously stirred at a temperature of 60 °C for 3 hours to encourage *in situ* crosslinking and the encapsulation of metal–organic frameworks (MOFs), leading to the development of a viscous gel-like substance. Consequently, the mass-based composition of the composite is represented by a Pd-MOF : CS : CMC : crosslinker ratio of approximately 1 : 2.5 : 2.5 : 2.5. This gel was then dispensed into molds or a Petri dish and subjected to freeze-drying. After forming the gel, the mixture was frozen at −80 °C for 12 hours for complete solidification. Following this, a lyophilization process produced a porous PMCC sponge structure. The freeze-drying occurred at −50 °C and 0.05 to 0.1 mbar for 24 hours, allowing gradual sublimation of water. The result was a highly porous, lightweight, and stable composite ideal for adsorption applications (Fig. 1).

2.3. Elimination and batch studies of the adsorption of CIP onto PMCC

A specified quantity of 0.02 g of the PMCC sponge was submerged in a ciprofloxacin (CIP) solution with concentrations ranging from 40 to 600 mg L^{-1} and a total volume of 25 mL in order to assess the adsorption isotherm. The solution pH was carefully adjusted to 8 through the addition of NaOH.[16,17] After that, the combination was put in a water bath oscillator with a thermostat that ran at 200 rpm and kept the temperature constant at 25 °C. To assess the adsorption characteristics, samples were carefully removed at predetermined intervals of 5 to 100 min. Following the centrifugation of the collected sample solutions, a UV-Vis spectrophotometer set to a wavelength of 272 nm was used to measure the CIP concentrations. The adsorption capability (q_e, mg g^{-1}) and the removal efficacy of the ciprofloxacin antibiotics (R, presented as a percentage) were determined based on eqn (1) and (2), respectively:

$$q_e = \frac{(C_0 - C_e)V}{M} \quad (1)$$

$$\%\ R = \frac{(C_0 - C_t)}{C_0} \times 100 \quad (2)$$

This analysis measures the CIP solution's initial concentration (C_0), as well as the equilibrium concentration (C_e), both of which are given in mg L^{-1}. The CIP solution's entire volume, expressed in mL, is represented by the variable V. Furthermore, m, which is measured in mg, represents the mass of the PMCC that was used as the adsorbent. The percentage of CIP that has been removed from the solution is indicated by the removal efficiency of CIP or R (%). The pH values of the antibiotic solution were systematically attuned between 3 and 10 in order to assess the impact of pH on the adsorption capacity of the material. For the experiment, 25 mL of the CIP solution with a concentration of 400 mg L^{-1} was mixed with 0.02 g of PMCC. This suspension was then disturbed in a thermostatically regulated water bath at a speed of 250 rpm while preserving a constant temperature of 25 °C for 60 min. After this period of agitation, the samples were filtered, and the quantities of CIP in the resultant solutions were analyzed using UV spectrophotometry.[18] The determination of the adsorption capability was achieved utilizing eqn (1). To assess the kinetics of adsorption, 0.02 g of PMCC was added to each substance bottle covering 25 mL of a 400 mg per L CIP solution, which was maintained at a pH level of 8 throughout the adsorption experimentations. The samples were agitated at a controlled speed of 250 rpm at 25 °C for different durations, exactly from 0 to 100 min. After this process, the antibiotic concentration was quantified to assess the impact of the treatment.[19,20] The adsorption capacity was quantified, as outlined in eqn (1). In the context of the thermodynamic analyses, 0.02 g of the PMCC was added to each reagent container, each holding 25 mL of CIP with a concentration of 400 mg L^{-1}, which was specifically attuned to a pH level of 8. These experiments were performed at three distinct temperatures: 288, 298, and 308 K, while ensuring that each test maintained a uniform duration of 60 min. Following that,

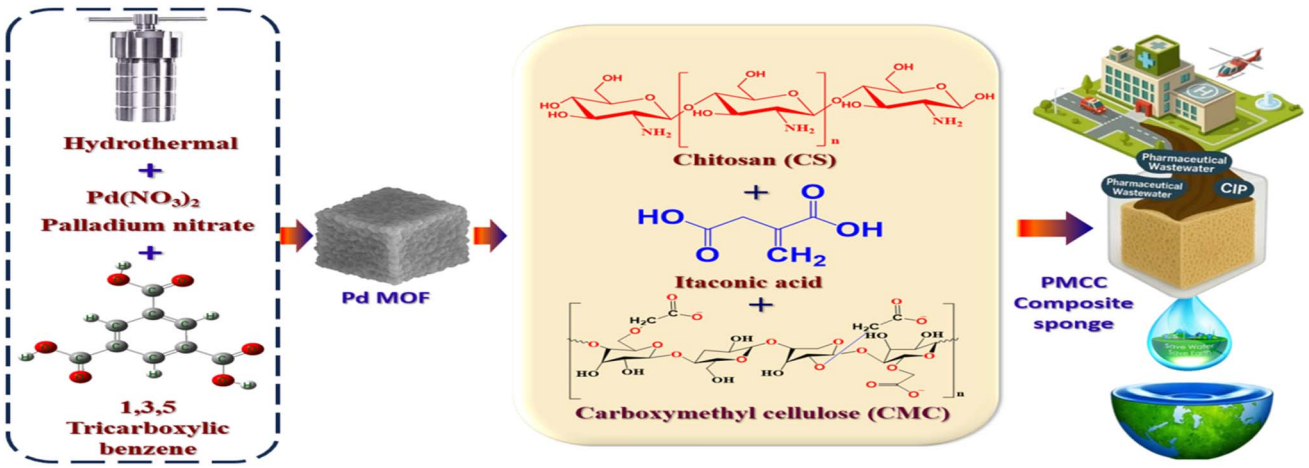

Fig. 1 Visual illustration of the PMCC production.

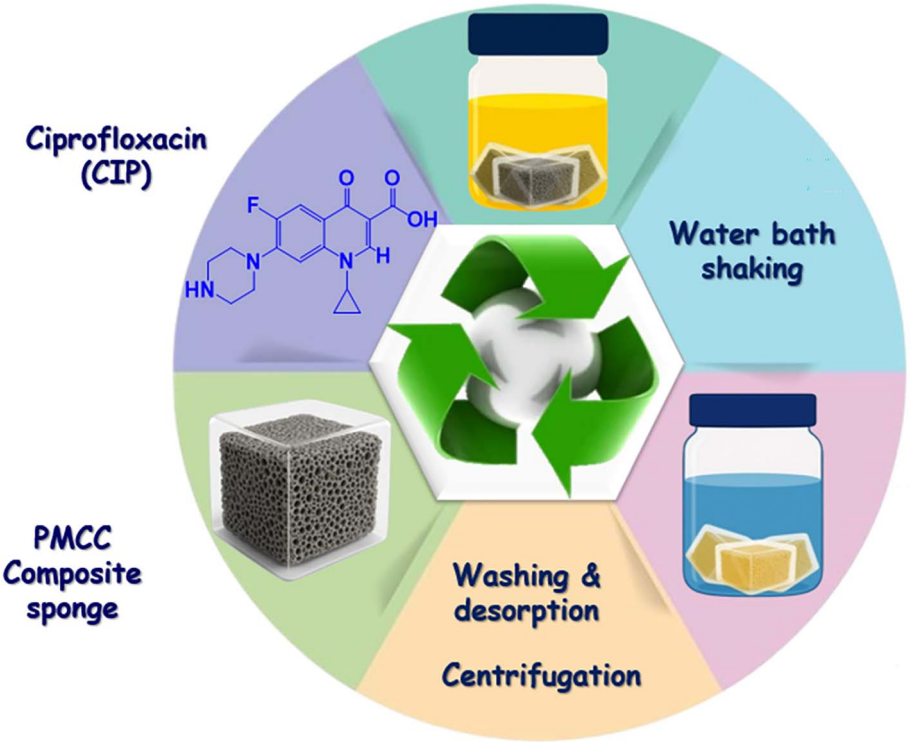

Fig. 2 Diagrammatic representation of the adsorption and removal of CIP by PMCC.

appropriate mathematical formulas were used to extract the pertinent thermodynamic limits (Fig. 2).

2.4. Investigational design

Within the domain of experimental plan, the Box–Behnken design (BBD) method is particularly distinguished for its effectiveness in performing comprehensive and methodical evaluations of specified outcomes. This methodology facilitates the development of a meticulously organized framework that aligns accurately with the collected data, thereby elucidating the underlying principles that regulate the independent variables in a specific manner, adsorbent quantity, pH level, and extent that are critical for achieving the main goal of the proposed response, which is the removal of CIP.[21] The present research is basically focused on conducting adsorption experiments guided by the BBD framework, which is effectively facilitated using Design-Expert software (Stat-Ease, Version 13). The dataset lists the different factor stages under analysis and the codes associated with each level.[22] Eqn (3) describes the use of a second-degree quadratic model, which is a crucial component of this approach. The framework provided by this model allows the independent factors and the dependent result to work together:

$$Y = \beta_o + \sum \beta_i X_i + \sum \beta_{ii} X_i^2 + \sum\sum \beta_{ij} X_i X_j \quad (3)$$

In this state, Y signifies the desired result, precisely the CIP, while X_i and X_j represent the variables examined. The resulting elimination process is characterized by a systematic interaction involving 17 carefully structured experiments (Table S3). A carefully measured amount of the PMCC was mixed with 25 mL of the CIP solution for each of the subsequent CIP removal tests.

Response Surface Methodology (RSM) serves as a robust framework for determining the optimal mixtures of numerous variables to improve experimental results. A significant technique based on the RSM is the BBD, which is distinguished by its use of first and second-order constants resulting from three-level partial factorial arrangements. This approach utilizes mathematical modeling for the ensuing analysis.[23] To illustrate this approach, a structured framework is introduced that analyzes the improvement in adsorption capacity in correlation with three specific variables: time, pH, and adsorbent quantity, as detailed in Table S4. Consequently, three analytical levels were examined: +1, 0, and −1. In summary, the RSM provides essential insights that facilitate the identification of the optimal solution for a given problem.[24]

3. Results and discussion

3.1. Characterization of PMCC

3.1.1. X-ray diffraction (XRD). The X-ray diffraction (XRD) pattern of PMCC exhibits a notable combination of both crystalline and amorphous features. The diffractogram reveals multiple well-defined and sharp reflections within the 2θ angle spectrum of 5° to 80°, with a significant peak observed around 33°, which is indicative of the crystalline planes of the original Pd-MOF. The identified reflections align closely with the reference pattern recorded for Pd-MOF, as reported by Espallargas *et al.*[25] with a reference to the following manuscript (https://pubs.rsc.org/en/content/articlelanding/2023/sc/d2sc05192c),

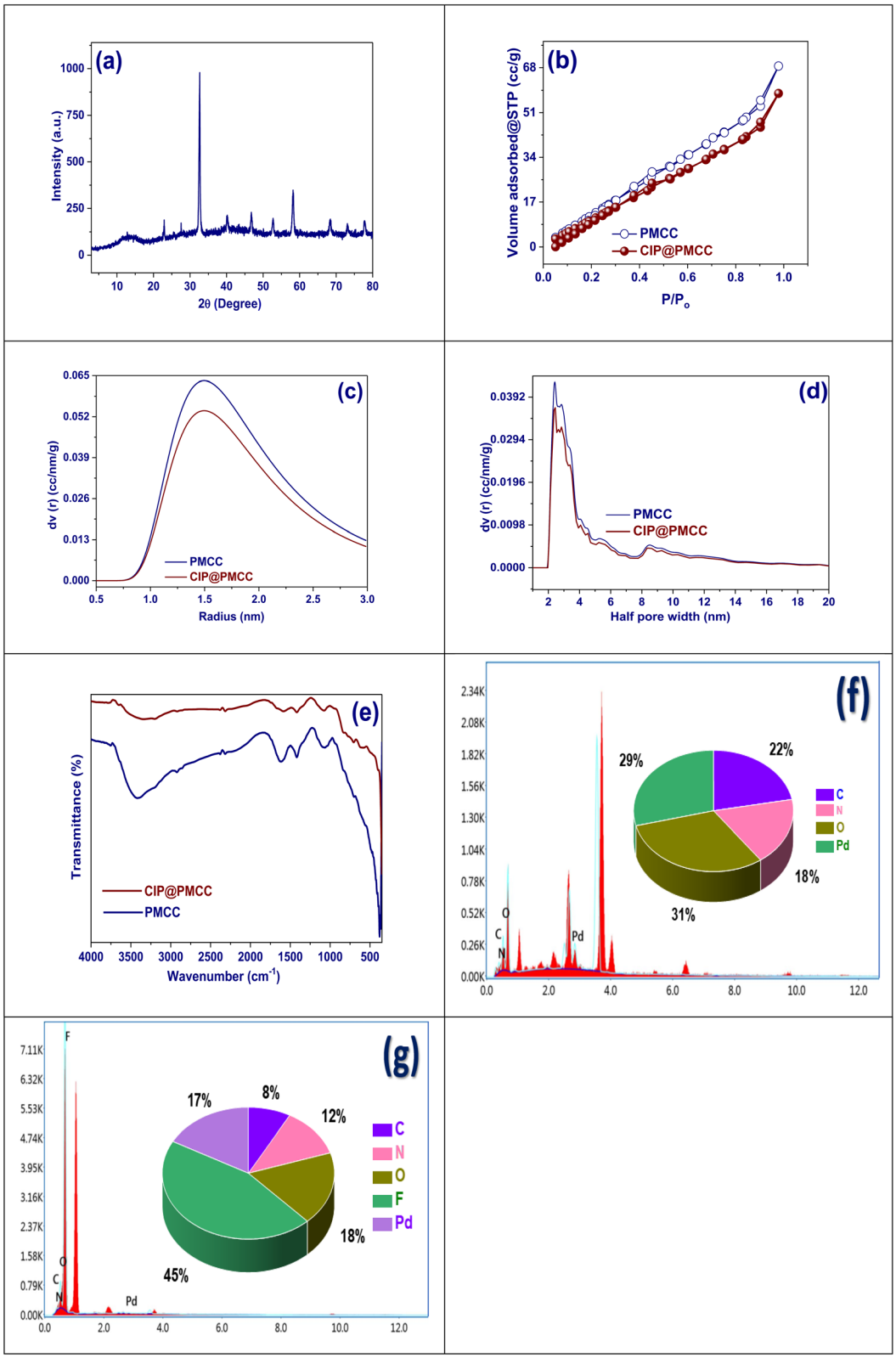

Fig. 3 (a) XRD pattern of PMCC, (b) N_2 adsorption/desorption isotherm of PMCC and CIP@PMCC, (c) pore-radius distribution, (d) pore-size distribution, (e) FTIR spectra of PMCC and CIP@ PMCC, (f) EDX spectra of PMCC, and (g) EDX spectra of CIP@ PMCC.

demonstrating that the long-range order of the MOF is preserved after encapsulation. Additionally, the presence of other peaks detected within the 10° to 60° range further indicates the retention of the ordered lattice structure of the MOF. Conversely, the broad diffuse halo observed below 10° is typical of amorphous biopolymers and is ascribed to the CS-

CMC matrix, which inherently lacks a defined crystalline arrangement. The concurrent existence of distinct MOF peaks alongside the amorphous polymeric background implies that the Pd-MOF crystallites maintain their structural integrity and are uniformly distributed within the polymer network. This preservation of crystallinity is crucial, given that the structural integrity of the MOF is intrinsically related to its adsorption and functional characteristics. The CCDC crystallographic reference included in this analysis serves as a verifiable benchmark, further affirming that the Pd-MOF phase is effectively retained within the PMCC (Fig. 3(a)).[25]

3.1.2. N_2 adsorption/desorption isotherm. The nitrogen adsorption–desorption isotherms for PMCC and CIP@PMCC show type-IV characteristics typical of mesoporous materials, indicated by a steady increase in nitrogen adsorption at lower pressures (P/P_0 < 0.2) and a sharp rise nearing $P/P_0 \approx 1.0$, reflecting capillary condensation. An H3-type hysteresis loop highlights the non-rigid plate-like particles that form slit-shaped pores. The PMCC sample demonstrates higher nitrogen adsorption capability with a BET surface area of 87.56 $m^2\ g^{-1}$, indicating a well-structured mesoporous network.[26] After the adsorption of CIP, the isotherm for CIP@PMCC shows a reduced adsorption volume and a decreased surface area of 68.6 $m^2\ g^{-1}$. This suggests that drug molecules occupied or hindered the mesoporous channels, indicating effective entrapment of CIP within the PMCC structure primarily through a pore-filling mechanism (Fig. 3(b)).

The analysis of the pore architectures in PMCC and CIP@PMCC sponges, exposed in Fig. 3(c and d), reveals the effect of CIP adsorption on the porous geometry. In Fig. 3(c), PMCC exhibits a peak in pore radius at 2.34 nm, confirming its mesoporous nature. After CIP adsorption, this peak shifts to around 1.96 nm, suggesting that the drug molecules occupied the pores. Fig. 3(d) shows a broad half-pore width distribution for PMCC, marked by a sharp peak between 2 and 4 nm and a tail extending to 20 nm, indicating a varied mesoporous structure.[27] After the ciprofloxacin loading, the overall pore distribution shows a slight shift toward smaller dimensions and reduced peak intensities (Table S5). The total pore volume drops from 0.12 $cm^3\ g^{-1}$ in PMCC to 0.088 $cm^3\ g^{-1}$ in CIP@PMCC, confirming successful CIP adsorption in the porous matrix. This results in decreased accessible pore volume and average pore radius, highlighting effective drug encapsulation within the PMCC mesoporous structures through a pore-filling mechanism (Table S6).

3.1.3. FT-IR. The FT-IR spectra of PMCC and CIP@PMCC sponges reveal distinct vibrational features that confirm the composite's structural consistency and its interaction with CIP. The PMCC spectrum shows a broad absorption band around 3400 cm^{-1}, linked to O–H and N–H stretching from chitosan and carboxymethyl cellulose. Peaks near 2920 cm^{-1} represent C–H stretching, and the band at 1650 cm^{-1} indicates C=O stretching (amide I) and possible N–H bending, signifying organic linkers and polymer structures.[28] A significant absorption feature at approximately 1570 cm^{-1} is linked to the stretching vibrations of C=N or aromatic C=C bonds from the Pd-MOF. The spectral area around 1400 and 1300 cm^{-1} indicates C–N stretching and O–H bending. The peak around 1050 cm^{-1} is linked to C–O–C and C–O stretching from the polysaccharide support. Metal–oxygen interactions are suggested by absorption features in the 500–700 cm^{-1} range, associated with Pd–O vibrations. After CIP adsorption, the CIP@PMCC spectrum shows notable variations: the comprehensive O–H/N–H band slightly widens and shifts, representing hydrogen bonding; the C=O stretching near 1650 cm^{-1} decreases or shifts due to the interaction with CIP's carboxylic groups; and new or enhanced bands in the 1700–1500 cm^{-1} region are linked to vibrations from the drug's aromatic and quinolone rings. Additionally, observed changes in the 1300 to 1000 cm^{-1} fingerprint region suggest interactions between CIP's functional groups and the polymer matrix, confirming successful CIP encapsulation in PMCC through electrostatic attraction and hydrogen bonding (Fig. 3(e)).

3.1.4. EDX. The Energy Dispersive X-ray (EDX) study of the PMCC shows the elemental composition and integration of key components. The spectrum discloses significant peaks for carbon (C), nitrogen (N), oxygen (O), and palladium (Pd), indicating organic polymers and metal centers. Carbon (22%) and nitrogen (18%) are associated with chitosan and carboxymethyl cellulose, while oxygen (31%) originates from hydroxyl, carboxyl, and ether groups in the matrix.[29] Palladium comprises 29% of the total elemental makeup, indicating effective immobilization within the composite sponge. The distinct Pd peaks in the low keV range confirm its high loading and even distribution. A pie chart exemplifies the balanced distribution of the four key elements, highlighting the hybrid organic–inorganic nature of the PMCC material, pointing to potential uses in drug loading, catalysis, or environmental remediation (Fig. 3(f)).

The EDX spectrum of CIP@PMCC, shown in Fig. 3(g), confirms the elemental arrangement after ciprofloxacin (CIP) incorporation and reveals significant changes from the original PMCC. The spectral data indicate specific signals for C, N, O, Pd, and F, with fluorine being a key indicator of ciprofloxacin due to its unique fluorinated structure. Fluorine has the highest atomic percentage at 45%, supporting the successful incorporation of CIP into the composite structure.[30] The carbon (8%), nitrogen (12%), and oxygen (18%) contents align with the biopolymeric structure of chitosan and carboxymethyl cellulose, including functional groups like carboxylic, ketone, and amine in CIP. A 17% palladium retention suggests that the framework remains intact after drug incorporation. The pie chart shows compositional changes following CIP encapsulation, highlighting the presence of fluorine, which is absent in PMCC. These results, alongside Pd signals, affirm the successful CIP adsorption in the PMCC sponge, boosting drug delivery and controlled release functions.

3.1.5. SEM. Fig. 4(a) illustrates the SEM-EDX mapping of the PMCC, showcasing a highly porous and rough surface with irregularly aggregated particles. This morphology enhances the surface area and offers abundant active sites for efficient adsorption, facilitating the effective capture and retention of CIP from aqueous media.[31] EDX mapping confirms a uniform distribution of carbon (24%), nitrogen (16%), oxygen (28%), and

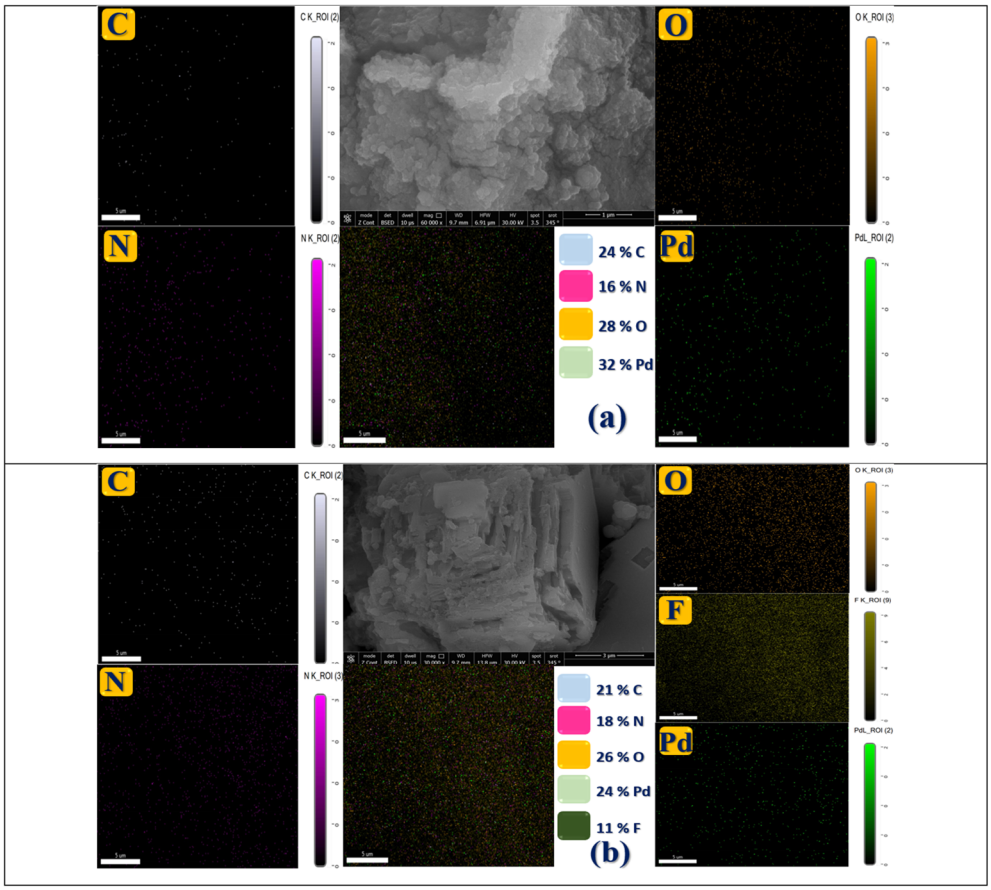

Fig. 4 SEM-EDX mapping of (a) PMCC and (b) CIP@PMCC.

palladium (32%) in the composite. Functional groups like –NH_2, –COOH, and –OH from nitrogen and oxygen promote hydrogen bonding and electrostatic interactions with CIP. The dispersed palladium enhances coordination interactions, increasing the CIP adsorption affinity. This sponge-like matrix validates PMCC's effectiveness in removing ciprofloxacin from wastewater.

Fig. 4(b) displays a SEM-EDX mapping image of CIP@PMCC, highlighting the adsorption of CIP on PMCC through its morphological and elemental attributes. The SEM image reveals a dense, crystalline-like surface, contrasting the more porous unloaded PMCC, indicating that CIP molecules have filled the pores or coated the sponge surface. EDX analysis shows an unvarying distribution of elements: carbon (21%), nitrogen (18%), oxygen (26%), palladium (24%), and fluorine (11%). The presence of fluorine, absent in PMCC, confirms the incorporation of CIP due to its fluorinated quinolone structure. The even distribution, especially of fluorine and nitrogen, indicates that CIP has adhered to the surface and possibly engaged in interactions like hydrogen bonding and electrostatic forces. This examination underscores PMCC's capacity to efficiently adsorb CIP from aqueous solutions, making it a promising option for removing pharmaceutical contaminants from wastewater.

3.1.6. XPS analysis. The high-resolution XPS C 1s spectra of PMCC and CIP@PMCC reveal significant evidence about the surface chemical configuration and functional groups involved in the CIP adsorption.[32] In the PMCC C 1s spectrum, three peaks are present. The chief peak at 284.87 eV (45.53%) corresponds to the C–C/C=C bonds in the carbon backbone. The second peak at 285.90 eV (40.88%) is attributed to the C–O or C–N bonds, indicating the presence of functional groups like hydroxyl or amine from cellulose or modifications. A smaller peak at 286.26 eV (13.59%) is linked to C=O or O–C–O groups, corresponding to oxidized carbon species. The C 1s spectrum of CIP@PMCC shows changes in peak positions and intensities due to ciprofloxacin adsorption. A new peak appears at 288.13 eV (59.02%) for the O=C–O and –COOH groups from ciprofloxacin. The C–C/C=C peak decreases to 18.01% at 285.30 eV, and the C–O/C–N peak shifts slightly to 285.90 eV at 22.97%. These changes confirm ciprofloxacin's immobilization on the PMCC surface, highlighting the drug-functional group interactions through hydrogen bonding or coordination with oxygen groups (Fig. 5).

The XPS N 1s spectra of PMCC and CIP@PMCC reveal significant changes in the nitrogen chemical environments after ciprofloxacin incorporation. In the PMCC spectrum, two peaks are observed: the first at 400.88 eV (31.88%) corresponds to amine or pyrrolic nitrogen species (–NH or –N–), linked to nitrogen-doped carbon or natural polymer backbones. The second peak at 401.21 eV (68.12%) indicates protonated or

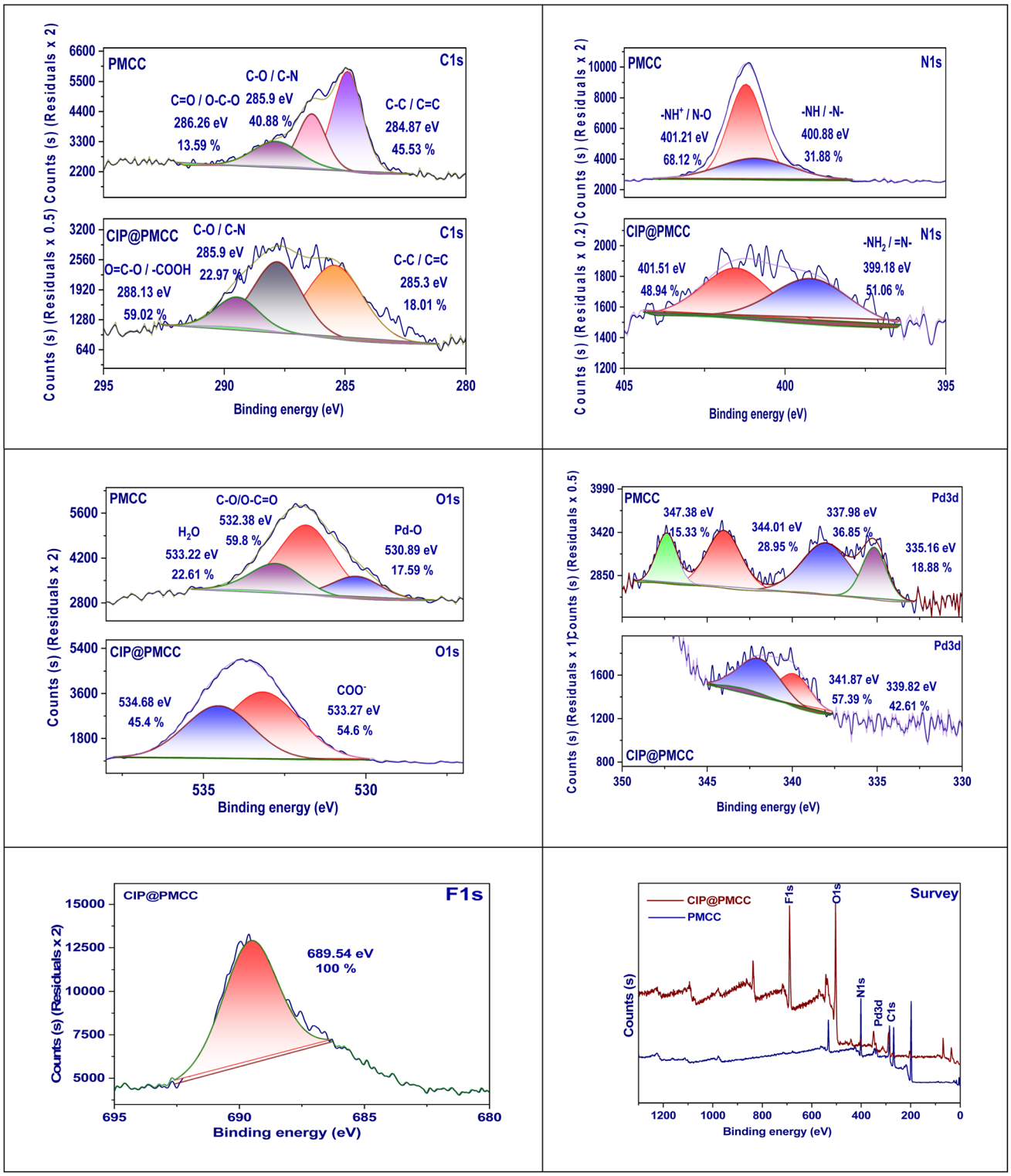

Fig. 5 XPS spectra of PMCC and CIP@ PMCC.

oxidized nitrogen species, suggesting surface modifications or partial oxidation of nitrogen functionalities within the PMCC framework.[33] CIP@PMCC's N 1s spectrum shows notable changes after ciprofloxacin adsorption, including a new peak at 399.18 eV, which constitutes 51.06% of the total area, attributed to neutral amine or imine nitrogen (–NH_2 or =N–) from ciprofloxacin. The second peak shifts to 401.51 eV, contributing 48.94%, indicative of protonated nitrogen or nitrogen involved in strong hydrogen bonding or electrostatic interactions. These changes confirm effective ciprofloxacin immobilization on

PMCC with new nitrogen functionalities and shifts in binding energies, reflecting strong chemical interactions, like hydrogen bonding or charge-assisted complexation, between the drug and nitrogen-rich material sites.

The XPS O 1s spectra of PMCC and CIP@PMCC reveal significant changes in the chemical environment due to CIP adsorption. In PMCC, three peaks appear at binding energies of 530.89 eV (17.59%), 532.38 eV (59.8%), and 533.22 eV (22.61%). The peak at 530.89 eV indicates lattice oxygen or metal–oxygen bonds, while the predominant peak at 532.38 eV relates to hydroxyl or carboxylic groups. The component at 533.22 eV suggests adsorbed water or weakly interacting oxygen species. Following CIP adsorption, CIP@PMCC shows two main peaks at 533.27 eV (54.6%) and a new peak at 534.68 eV (45.4%).[34] The intensified 533.27 eV peak reveals a strong interaction between CIP and surface hydroxyl or carboxyl groups, likely through hydrogen bonding or electrostatic attraction. The 534.68 eV peak indicates oxygen in electron-withdrawing environments from carboxyl and ketone groups, confirming CIP's adsorption and changes in surface oxygen species, showcasing chemical interactions with the PMCC matrix (Fig. 5).

The assertion of a $Pd^0 \rightarrow Pd^{2+}$ transformation occurring after ciprofloxacin (CIP) adsorption has been retracted, as such a reaction is not justifiable under the mild adsorption conditions employed, and ciprofloxacin does not possess the requisite oxidative strength to catalyze this conversion. To rectify the interpretation, all high-resolution Pd 3d spectra were re-fitted in accordance with established XPS protocols corroborated by the literature: the C 1s hydrocarbon peak was calibrated to 284.8 eV, the spin orbit splitting for Pd 3d was constrained to approximately 5.26 eV, the area ratio for $3d_{5/2}$ to $3d_{3/2}$ was preserved at 3 : 2, and the full width at half maximum values were confined to ranges in agreement with documented references for both Pd^0 and Pd^{2+}. Standard binding energy values from the literature (Pd^0 $3d_{5/2}$ ≈ 334.6–335.2 eV; Pd^{2+} ≈ 336.3–337.0 eV) guided the fitting process. The revised fittings reveal that both PMCC and CIP@PMCC consist of a combination of metallic (Pd^0) and oxidized (Pd^{2+}) palladium species, with only negligible shifts (<0.5 eV) observed post CIP adsorption. These minor deviations are interpreted as arising from the ligand–metal coordination effects rather than redox reactions. Moreover, the X-ray diffraction (XRD) patterns obtained before and after CIP adsorption displayed consistent peak positions and intensities, thereby corroborating that the crystalline structure of the Pd-metal–organic framework (MOF) remains intact and is not subject to structural alterations induced by oxidation. To enhance transparency and adhere to best practices, complete XPS survey spectra encompassing the full range for both PMCC and CIP@PMCC, including the corresponding XPS-derived surface atomic percentages, have been included in the SI section, thereby providing comprehensive validation of the elemental composition and binding energy assignments (Fig. 5).

The XPS spectrum of CIP@PMCC shows the effective adsorption of CIP on PMCC through detectable fluorine. A sharp peak at a binding energy of 689.54 eV indicates 100% F 1s signal intensity, indicative of fluorine in a highly electronegative environment, related to C–F bonds, crucial to the ciprofloxacin molecule.[35] The strong F 1s signal, absent in the unmodified PMCC, confirms ciprofloxacin's immobilization on the composite surface. Its well-defined shape indicates a uniform chemical environment for fluorine, supporting that ciprofloxacin is effectively adsorbed onto the PMCC matrix through stable interactions, without significant degradation or alteration of the fluorine-containing groups.

The XPS survey spectrum reveals the surface elemental configurations of PMCC (blue line) and CIP@PMCC (red line), highlighting the adsorption of CIP onto the composite. In the PMCC spectrum, distinct peaks are noted: C 1s around 285 eV, O 1s near 532 eV, N 1s at approximately 400 eV, and Pd 3d from 335 to 345 eV, representing carbon, oxygen, nitrogen from organic components, and palladium within the composite. After combining with ciprofloxacin, distinct alterations arise in the CIP@PMCC spectrum. Notably, a strong F 1s peak at around 689 eV appears, confirming fluorine's presence from the ciprofloxacin's fluorinated aromatic ring. There is also a significant rise in the N 1s peak intensity, reflecting contributions from nitrogen-rich functional groups in ciprofloxacin, such as amine and heterocyclic groups.[36] Minor enhancements in the O 1s and C 1s signals indicate the occurrence of surface interactions and the formation of complexes between the drug and the functional groups present in the composite (Table S7). Taken together, these spectral features affirm the effective immobilization of ciprofloxacin onto PMCC and underscore the compositional and chemical alterations that transpire as a result of the adsorption procedure, as demonstrated in Fig. 5.

3.1.7. Zero point of charge. Fig. 6(a) demonstrates the determination of the zero point of charge (pH_{zpc}) for the PMCC sponge, recognized at a pH of 4.39, where the change in pH (ΔpH) is zero. This pH value represents the state in which there is no net electrical charge on the sponge's surface. The surface has a positive charge once the pH is less than 4.39 and a negative charge whenever the pH is higher. This point plays a serious role in the adsorption efficiency of CIP, an antibiotic that can exist in various ionic states based on pH levels. At pH values above 4.39, the negatively charged PMCC surface promotes electrostatic attraction to the positively charged CIP, thereby enhancing its adsorption and removal from water.[37] In contrast, at pH levels below 4.39, the electrostatic repulsion between the equally charged PMCC surface and CIP diminishes the effectiveness of adsorption. Consequently, maintaining a pH above the pH_{zpc} considerably improves the PMCC capability to remove ciprofloxacin from aqueous solutions.

3.2. Batch experimentations

3.2.1. Effect of pH. The impact of pH on the adsorption capacity (q_e) of CIP on the PMCC, shown in milligrams of CIP adsorbed by a gram of adsorbent, is demonstrated by the preceding bar graph. The adsorption capacity exhibits a consistent increase as the pH progresses from 3 to 8, reaching a peak around pH 8 with a maximum q_e of approximately 450 mg g^{-1}. This pattern signifies how pH affects both the surface charge of the PMCC sponge and the ionization state of

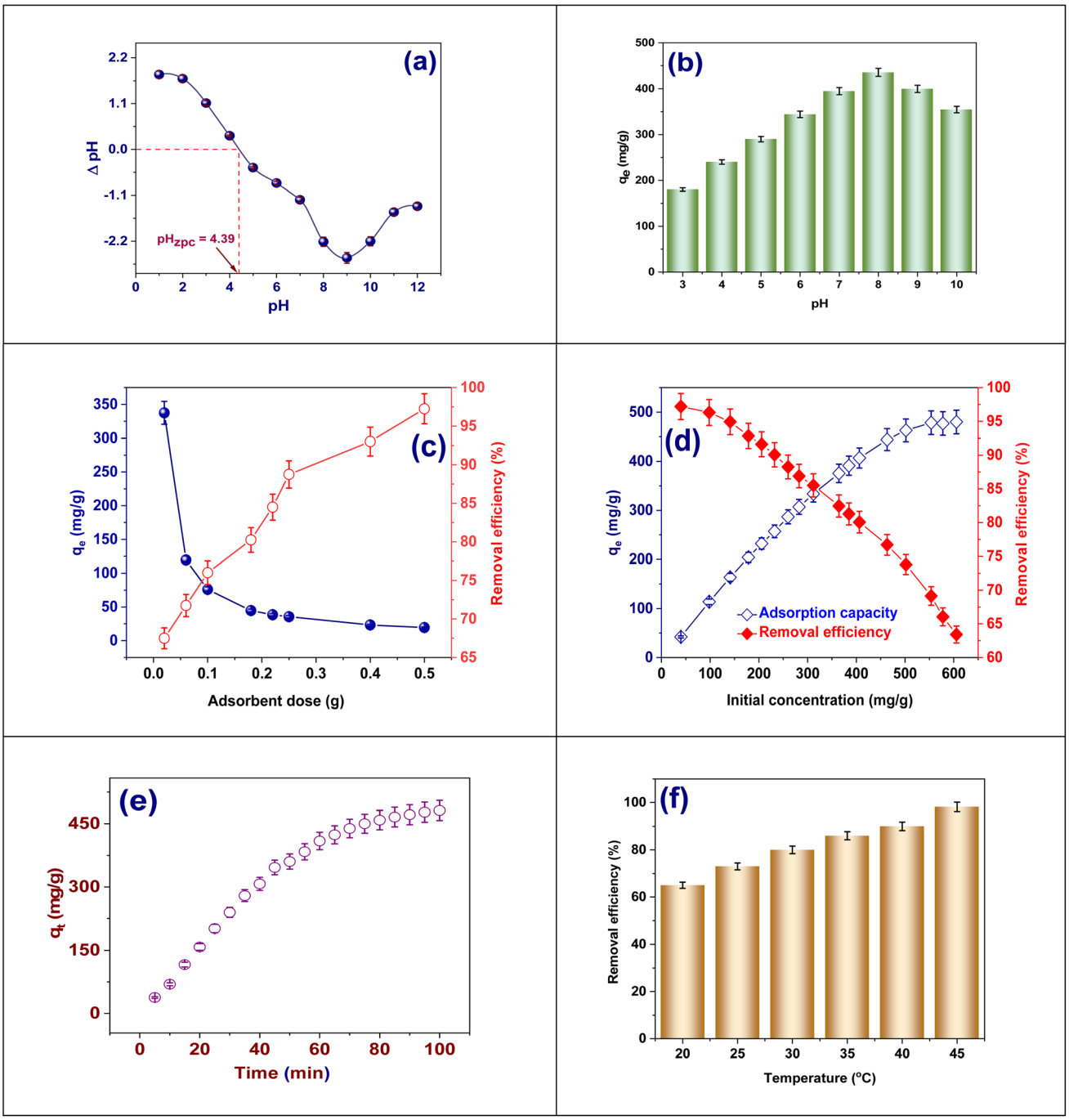

Fig. 6 (a) Calculation of the pH_{zpc} of PMCC, (b) effect of the pH on the adsorption efficiency of CIP on PMCC, (c) effect of the adsorbent dose on adsorption capacity and removal efficiency, (d) effect of the initial concentration of CIP on adsorption capacity and removal efficiency, (e) effect of interaction time on adsorption capacity, and (f) effect of temperature on removal efficiency.

CIP. At lower pH levels (3–5), the surface of the sponge carries a positive charge (as indicated by a pH_{zpc} of approximately 4.39), resulting in electrostatic repulsion with the cationic form of CIP, leading to diminished adsorption. As the pH exceeds the pH_{zpc} value, the sponge's surface becomes negatively charged, facilitating stronger electrostatic attraction to the positively charged CIP molecules, thereby increasing adsorption. The peak adsorption detected at pH 8 indicates that this pH level presents the most conducive conditions for CIP removal, likely because the zwitterionic or cationic form of CIP is predominant, which interacts robustly with the negatively charged surface of the PMCC.[38] However, beyond pH 8, a small decline in adsorption capability occurs, likely owing to the increasing creation of anionic CIP species that experience lower attraction or even repulsion from the similarly charged surface (Fig. S1). Consequently, pH is a critical factor influencing the adsorption efficiency of CIP on the PMCC (Fig. 6(b)).

3.2.2. Effect of dose. Using the PMCC, Fig. 6(c) exemplifies how the adsorbent amount affects the adsorption capacity (q_e, mg g^{-1}) and effectiveness of removal (%) of CIP. The graph features two vertical axes: the left axis (in blue) indicates q_e, while the right axis (in red) illustrates the removal efficiency. As the adsorbent dose increases from 0.05 to 0.5 g, q_e experiences a notable decline, whereas the removal efficiency shows a consistent increase. At lower dosages, such as 0.05 g, the concentration of available CIP is focused on a limited number of active sites, leading to a higher adsorption per gram of sponge (with q_e exceeding 350 mg g^{-1}).[39] However, with increased dosage, the same quantity of CIP is distributed over a greater surface area of the adsorbent, which decreases the adsorption per gram owing to the saturation of active sites and potential aggregation of particles that limits surface availability. In contrast, removal efficiency sees a significant rise, nearing 100% at the maximum dose of 0.5 g, suggesting that a greater amount of adsorbent provides more active sites, facilitating enhanced CIP removal from the solution. This inverse correlation illustrates a crucial balance: while higher dosages enhance removal efficiency, they simultaneously diminish specific adsorption capacity. Therefore, identifying the optimal adsorbent dose is contingent upon whether the application aims for maximum efficiency or maximum adsorption capacity per unit mass of the adsorbent.

3.2.3. Effect of the CIP concentration. Fig. 6(d) illustrates how the original concentration of ciprofloxacin (CIP) affects the adsorption properties of the PMCC. There is a pronounced inverse correlation between the adsorption capacity (q_e, mg g^{-1}) and the removal efficacy (%). As the initial CIP concentration increases from 0 to 600 mg L^{-1}, the adsorption capacity experiences a notable increase, surpassing 500 mg g^{-1} at the maximum concentration.[40] This pattern can be explained by the heightened concentration gradient, which promotes the mass transfer of CIP molecules towards the sponge's surface, resulting in a higher number of adsorption sites being occupied. In contrast, the removal efficiency decreases gradually, diminishing from nearly 100% at lower concentrations to about 60% at 600 mg L^{-1}. This decline in efficiency is linked to the capacity of active seats on the sponge; despite a higher absolute quantity of CIP being adsorbed, a substantial amount remains in the solution as the available surface becomes completely utilized. These findings indicate that while elevated initial concentrations boost adsorption capacity, they concurrently reduce the overall removal efficiency, underscoring the necessity to balance these factors according to specific application objectives.

3.2.4. Effect of contact time. The impact of contact time on the CIP adsorption by the PMCC is shown in Fig. 6(e), which also exemplifies the relationship between duration (min) and adsorption capability (q_t, mg g^{-1}). The data reveal a swift rise in adsorption through the initial moments, particularly in the first 30 min, which signifies that a substantial number of active seats on the sponge's surface is easily accessible for CIP adsorption. Following this initial spike, there is a more gradual rise in adsorption from 30 to 100 min, indicating that over time, the available sites for adsorption become increasingly saturated, leading the system to approach an equilibrium state. The plateau observed after around 80 min suggests that the adsorption process has nearly reached equilibrium, with only a minor increase in q_t, stabilizing at approximately 450 mg g^{-1}. This trend aligns with the conventional adsorption process, where a strong affinity between the adsorbent and adsorbate leads to a rapid initial uptake, succeeded by a slower phase limited by diffusion. Overall, these findings indicate that the PMCC demonstrates high efficiency in removing CIP, with the majority of adsorption occurring in a brief contact time, rendering it effective for quick water treatment.[40]

3.2.5. Effect of temperature. The bar graph depicted in Fig. 6(f) exemplifies the effect of temperature on the efficiency of CIP removal by the PMCC. The data specify a consistent rise in the elimination efficacy as the temperature rises, starting from about 70% at 20 °C and reaching nearly 100% at 45 °C. This pattern signifies that the adsorption of CIP onto the PMCC sponge is an endothermic process, where higher temperatures facilitate enhanced adsorption. The elevation in temperature likely increases the kinetic energy of the CIP particles, which improves their diffusion rate toward the sponge surface, thus promoting greater contact with active adsorption sites. Furthermore, higher temperatures may contribute to increased porosity or elasticity of the sponge matrix, enhancing access to internal binding sites. This temperature-dependent behavior emphasizes the potential for improved CIP removal in warmer environments and highlights the thermodynamically favorable characteristics of the adsorption procedure. In conclusion, the results indicate that the PMCC performs more effectively at higher temperatures, making it a feasible selection for CIP removal across different thermal scenarios.[41]

3.3. Adsorption isotherm

Adsorption isotherm models are necessary to comprehend the mechanics and effectiveness of CIP adsorption onto PMCC. These models facilitate the examination of surface characteristics, adsorption capacity, and interaction dynamics. They provide a framework for assessing how CIP molecules interact with the composite at equilibrium, which is important for accurately predicting performance and enhancing action procedures. The model of Langmuir isotherm determines the maximum adsorption capacity and uniformity in site behavior by assuming monolayer adsorption on a uniform surface.[42] On the contrary, the Freundlich isotherm defines multilayer adsorption on diverse surfaces with varying energy levels at binding sites.[43] The Dubinin–Radushkevich (D–R) model helps distinguish among chemical and physical adsorption processes by providing information on the energy required in adsorption and the porous properties of the sponges.[44] Additionally, the Temkin isotherm takes into account the connections among the adsorbent, as well as the adsorbate, highlighting the decrease in adsorption heat as the surface exposure increases.[45] Meanwhile, the Jossens model reports the complexities of heterogeneous surface characteristics, and the Toth isotherm provides a versatile fit over a broad range of concentrations, integrating

features from both the Langmuir and the Freundlich models.[46] Collectively, these isotherm models serve as important tools for assessing the adsorption behavior of CIP on PMCC sponges, important for the expansion of actual and scalable water-purification systems (Tables S8 and S9).

To comprehend the adsorption actions of CIP onto the PMCC, isotherms of adsorption models are essential. These models offer insights into how CIP interacts with the composite's surface when equilibrium is reached, allowing for a quantitative valuation of adsorption capability, surface properties, and interaction mechanisms, which are vital for developing effective water-treatment systems.[42] The Langmuir isotherm model, in particular, suggests that adsorption occurs as a monolayer on a uniform surface through a limited number of identical sites. Investigation of the data discloses that the model of Langmuir aligns carefully with experimental findings; the observed maximum adsorption capacity ($q_{m,exp} = 480.5$ mg g^{-1}) is nearly equivalent to the value computed *via* the Langmuir model ($q_m = 482.6$ mg g^{-1}). The Langmuir binding constant ($K_L = 0.034$ L mg^{-1}) indicates the strength of the interaction between the CIP particles and the surface. The adsorption process appears to be highly promising, as indicated by the infinite separation factor ($R_L = 0.115$), which falls within the range of 0 to 1. These findings affirm that the PMCC sponge offers a robust and consistent binding environment for CIP and further validate the Langmuir model as an actual method for predicting and enhancing CIP adsorption under various scenarios (Table S10).

Adsorption isotherm models are crucial for comprehending the contact mechanisms between CIP and the PMCC, facilitating an in-depth examination of adsorption performance and surface properties.[43] The Freundlich isotherm model is one of these models that works well for systems with heterogeneous surfaces and multilayer adsorption.[43] The Freundlich model considers the different affinities that exist throughout the adsorbent surface, in contrast to the Langmuir model, which assumes uniform sites of adsorption. The parameters indicate that the Freundlich constant $n = 2.811$ suggests a favorable adsorption process, as n exceeds 1. This suggests that the PMCC exhibits a strong affinity for CIP and that the adsorption process is not confined to monolayer coverage. Furthermore, the constant $K_F = 78.39$ (mg g^{-1}) (L mg^{-1})$^{1/n}$ signifies both the adsorption capacity and strength, reinforcing the sponge's effectiveness across diverse concentration stages. The model's capability to describe adsorption on a variety of energetic sites renders it an essential tool for practical environmental applications, where surface irregularities and concentration gradients regularly occur. In summary, the Freundlich isotherm model significantly enhances the understanding of CIP adsorption behavior on PMCC, thereby supporting their development as versatile and efficient adsorbents (Fig. 7(a)).

Among these models, the isotherm model of Dubinin–Radushkevich (D–R) is particularly useful for differentiating between chemical and physical adsorptions. This is achieved by analyzing the adsorbent's porosity and energy characteristics. Unlike other models that presume uniform surface properties, the D–R model effectively handles heterogeneous surfaces and evaluates the potential energy associated with adsorption. The information indicates that the maximum adsorption capacity (Q_{DR}) is 423.26 mg g^{-1}, demonstrating the sponge's high capability to adsorb CIP. Additionally, the mean adsorption energy (E_a) is designed at 33.6 kJ mol^{-1}, suggesting that the

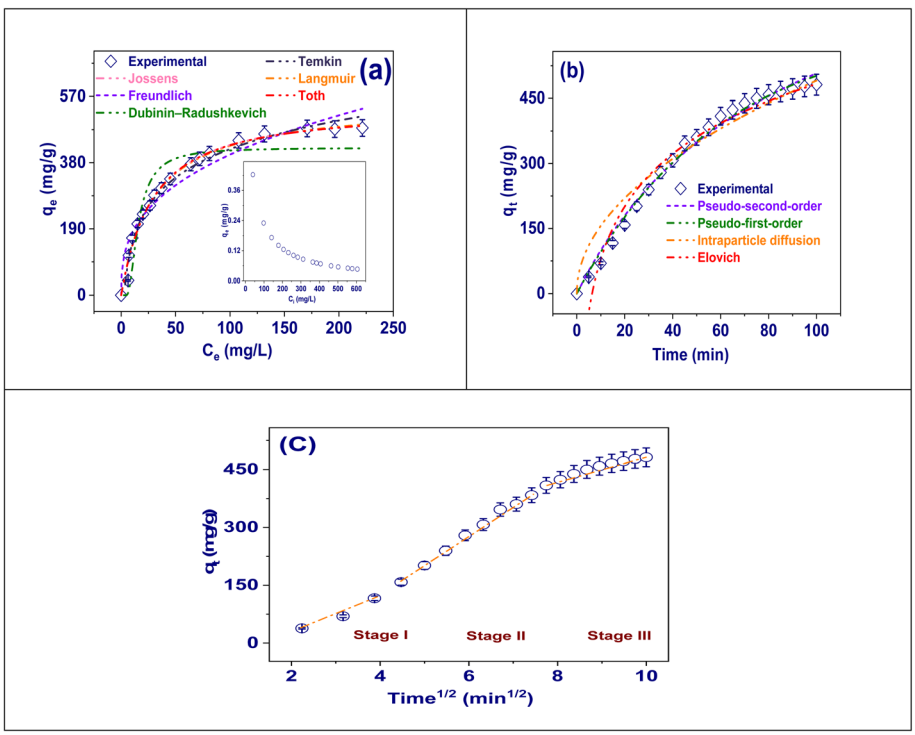

Fig. 7 (a) Isotherm models of adsorption, (b) kinetic models of adsorption, and (c) IPD model.

process of CIP adsorption on the PMCC is mainly chemical (chemisorption). This is supported by the fact that energy values exceeding 16 kJ mol^{-1} typically indicate robust chemical bonding rather than weak physical interactions. Furthermore, the constant K_{DR} illustrates the affinity and energy distribution present across the adsorbent. To summarize, the D–R isotherm model delivers critical images in the energy dynamics and mechanism behind CIP adsorption, underscoring the PMCC's potential in scenarios requiring strong and stable adsorption interactions.[44]

Adsorption isotherm models are essential tools for assessing and illustrating the interactions between CIP and the PMCC. They provide important information about the strength of adsorption and surface energetics. The Temkin isotherm model is especially significant because it considers the effects of indirect interactions involving the adsorbent and adsorbate and assumes that the heat of adsorption reduces linearly with increasing surface coverage. This distinction makes the model well-suited for schemes where the energy of adsorption varies, such as in heterogeneous materials like the PMCC sponge.[45] The information indicates that the Temkin binding energy constant (b_T) is 20.92 J mol^{-1}, which signifies the normal energy of CIP adsorption, suggesting a moderate level of binding interaction. Furthermore, the adsorption method appears to be advantageous based on the equilibrium binding constant (K_T) of 0.35 L mol^{-1}. These limits specify that the adsorption of CIP on the PMCC is characterized by strong connections between the adsorbent and adsorbate, potentially through forces like electrostatic or hydrogen bonding. Thus, the Temkin model provides illustrative insights into how these interactions shape the adsorption behavior, yielding a more comprehensive understanding of CIP uptake in PMCC sponges for real-world applications.[45]

One of them, the Jossens isotherm model, based on principles from statistical physics, is particularly effective for analyzing complex and heterogeneous adsorption systems, such as the PMCC. This model effectively addresses the variation in adsorption site energies and their distribution over the surface, making it ideal for materials with differing porosity and surface chemistry. The Jossens constants in the data, with values of $K = 17.89994$ and $J = 0.02732$, offer quantitative measurements of the interaction strength among the adsorbent and adsorbate, as well as the energy distribution among available binding sites. A high K value signifies a strong contact between CIP and the PMCC surface, while a low J value designates a diverse energy profile, suggesting that adsorption occurs across various types of sites. Implementing the Jossens model deepens the understanding of CIP adsorption under practical and variable surface conditions, highlighting the appropriateness of PMCC sponges for real-world applications where surface irregularities and complex adsorption dynamics are prevalent.[46]

Adsorption isotherm models play a vital role in analyzing and enhancing the adsorption procedure of CIP on PMCC, offering valuable information on adsorption capacity, surface interactions, and binding properties. In this context, the Toth isotherm model stands out as a flexible option that effectively integrates the key aspects of both the Langmuir and the Freundlich models, making it particularly applicable to systems with surface heterogeneity and non-ideal adsorption patterns. The Toth model presents a maximum adsorption capacity of $q_m = 536.30$ mg g^{-1}, signifying the strong affinity and high efficiency of the PMCC sponge for CIP. Furthermore, the equilibrium constant $K_T = 43.89$ L mg^{-1} indicates a favorable intensity of adsorption, while the exponent $t = 1.102$, which is nearly 1, suggests that the surface heterogeneity is moderate and that the adsorption behavior approaches that of Langmuir-type monolayer adsorption. The Toth model's capability to effectively represent adsorption across a broad concentration range enhances its significance for practical applications, ensuring that the adsorbent performance remains consistent in varying environmental scenarios. As a result, in addition to confirming the PMCC sponge's excellent performance, the Toth isotherm provides a complex and flexible framework for forecasting and enhancing its adsorption behavior under actual circumstances.[46]

3.4. Adsorption kinetics

Adsorption kinetic models are essential for understanding the processes and rate of CIP absorption onto PMCC. These models improve isotherm models by offering insights into the adsorption process's speed and routes. The pseudo-first-order model effectively characterizes the original phases of adsorption, where the rate relates to the number of available sites, a process often linked to physical adsorption.[47] However, a poor fit from this model may indicate that the adsorption involves more intricate mechanisms. Conversely, the pseudo-second-order model typically aligns more closely with the CIP adsorption data, suggesting that chemisorption, which entails stronger interactions, such as electron sharing or covalent bonding, is the primary mechanism.[48] This model also delivers a reliable estimate of the equilibrium capacity. The intraparticle diffusion model is involved in evaluating if pore diffusion in the PMCC acts as the rate-limiting factor.[49] It distinguishes various phases of adsorption, including external surface binding, gradual intraparticle diffusion, and the eventual establishment of equilibrium, thus emphasizing the complex, multi-stage processes that occur in porous materials. Finally, the Elovich model is particularly adept at depicting chemisorption on surfaces with energy heterogeneity, especially when adsorption rates decline over time due to site saturation or increased surface coverage.[50] Collectively, these kinetic models provide an in-depth understanding of the dynamics, rate-limiting steps, and interaction mechanisms of CIP with PMCC, making them essential for optimizing the performance of adsorption procedures in practical requests (Tables S8 and S9).

Important information about the early phases of the adsorption procedure can be gained from the pseudo-first-order kinetic model.[49] This model is particularly pertinent for describing physical adsorption throughout the initial interaction phase since it is founded on the idea that the adsorption rate is directly related to the quantity of accessible active sites on the adsorbent's surface. The data designates that the rate constant K_1 is 0.01684×10^{-2} min^{-1}, suggesting a comparatively slow rate of adsorption (Table S11). This might suggest

that the procedure is not solely administered by diffusion or that CIP molecules need additional time to effectively engage with the open sites. While this model may not represent the best fit for the entire adsorption timeframe, it successfully demonstrates how quickly the PMCC sponge can initiate CIP adsorption and reveals the accessibility of the surface sites. By contrasting the pseudo-first-order model with others, such as the pseudo-second-order model, researchers can classify whether the dominant interaction mechanism is physical or chemical, allowing for adjustments to system conditions for improved performance (Fig. 7(b)).

To illustrate the adsorption dynamics of CIP on PMCC, adsorption kinetic models, specifically the pseudo-second-order kinetic model, are quite helpful. This model provides a comprehensive knowledge of the mechanics and rate-limiting phases in the process of adsorption.[48] The adsorption type is primarily chemisorption, which entails distribution or exchanging of electrons among the adsorbent and the adsorbate. The data indicate a rate constant of $K_2 = 1.2798 \times 10^{-5}$ g mg^{-1} min^{-1} and a calculated equilibrium adsorption capacity of $q_e = 484.6$ mg g^{-1}, suggesting robust and efficient communication between the CIP and the PMCC surface (Table S11). The high equilibrium adsorption capacity is consistent with experimental findings, which supports the model's consistency in forecasting the adsorption behavior. The pseudo-second-order model is particularly adept for scenarios where chemical bonds are the main driving force, thus making it suitable for evaluating high-affinity adsorbents, such as PMCC. Additionally, this model enhances the project and scaling of adsorption schemes by emphasizing the kinetic control of the process over mere diffusion. In summary, the pseudo-second-order model offers a detailed comprehension of the adsorption kinetics, highlighting the effectiveness and appropriateness of PMCC sponges in removing CIP from water sources.

Using models of adsorption kinetics, particularly the intraparticle diffusion model, has proven extremely useful in explaining the multi-step mechanism for the adsorption of CIP onto PMCC.[49] These models assist in evaluating whether the transportation of CIP particles into the internal pores of the sponge serves as a key rate-limiting issue in the entire adsorption procedure. Data reveal that the intraparticle diffusion rate constant is $K_i = 48.994$ mg g^{-1} min$^{-1/2}$, and the boundary layer intercept is $X = 70.22$ mg g^{-1}. These values indicate that while intraparticle diffusion plays an important role in the adsorption process, it is not the only influencing factor, as evidenced by the non-zero intercept. The comparatively high K_i value suggests an effective diffusion rate within the sponge structure, whereas the intercept reflects the effects of boundary layer dynamics and external surface adsorption during the early phases of the process.[49] The model's capability to break down the adsorption into distinct stages of surface adsorption, pore diffusion, and equilibrium renders it a valuable resource for analyzing complex, porous materials, such as PMCC. In summary, the intraparticle diffusion model offers an understanding of how the sponge's structural characteristics affect the CIP removal efficiency and facilitates the advancement of adsorbents for water-treatment purposes (Fig. 7(b)).

The usage of adsorption kinetic models, particularly the Elovich model, holds noteworthy importance in illustrating the adsorption behavior of CIP on PMCC, notably within systems featuring chemically reactive and varied surfaces (Table S11). The Elovich model works under the premise that the adsorption rate declines exponentially as the surface becomes increasingly covered.[50] This characteristic makes it particularly suitable for representing chemisorption processes, where variations in surface energy lead to a diminishing availability of active locations. Based on the given parameters, the initial adsorption rate constant is $\alpha = 8.92358 \times 10^{-4}$ mg g^{-1} min^{-1}, while the constant of desorption is $\beta = 175.576$ g mg^{-1}. These values indicate an original phase of slow adsorption, which is followed by a swift rise in the surface resistance as the active sites become filled. The substantial β value suggests that CIP molecules encounter greater challenges in accessing available sites as time progresses, a phenomenon consistent with the characteristics of heterogeneous surfaces. Utilizing the model of Elovich in such scenarios is beneficial because it accommodates complex and energetically varied interactions, offering insights that more simplistic kinetic models fail to provide.[50]

3.5. Diffusion mechanism

The attached graph illustrates the intraparticle diffusion behavior of ciprofloxacin (CIP) adsorption onto the PMCC, with the adsorption capacity (q_t, mg g^{-1}) plotted against the square root of time (min$^{1/2}$). The curve is segmented into three separate stages (I, II, and III), each representing a specific mechanism in the adsorption procedure. Stage I is characterized by a sharp increase in q_t, representing the rapid adsorption on the outside surface of the sponge driven by boundary-layer diffusion. This is followed by Stage II, where the slope decreases, signifying a slower, diffusion-controlled process as the CIP particles enter the pores of the sponge matrix.[49] Lastly, Stage III displays a plateau, reflecting the attainment of adsorption equilibrium with minimal further uptake. It is inferred that the failure of the lines to pass into the origin hinders intraparticle diffusion, even if it is not the only rate-limiting mechanism. Rather, pore diffusion, surface contact, and possible structural changes inside the sponge all work together to control the adsorption process. This multi-phase profile confirms the complex and efficient adsorption mechanism of the PMCC for CIP removal (Fig. 7(c)).

3.6. Adsorption thermodynamics

An extensive examination of the temperature-dependent adsorption properties of CIP on the PMCC is provided by the figures, as well as thermodynamic data that are presented. As shown in Fig. 8(a), which employs the van't Hoff model, there is a direct linear overtone between $\ln K_C$ and $1/T$, suggesting that the adsorption process is influenced by temperature and allowing for the determination of key thermodynamic limits (Tables S8 and S9). Fig. 8(b) demonstrates the Arrhenius model, which reveals that as $1/T$ decreases, $\ln K_2$ increases, suggesting that higher temperatures lead to a faster adsorption rate, revealing the thermally activated nature of the chemisorption process.[50] Furthermore, the idea that adsorption is spontaneous

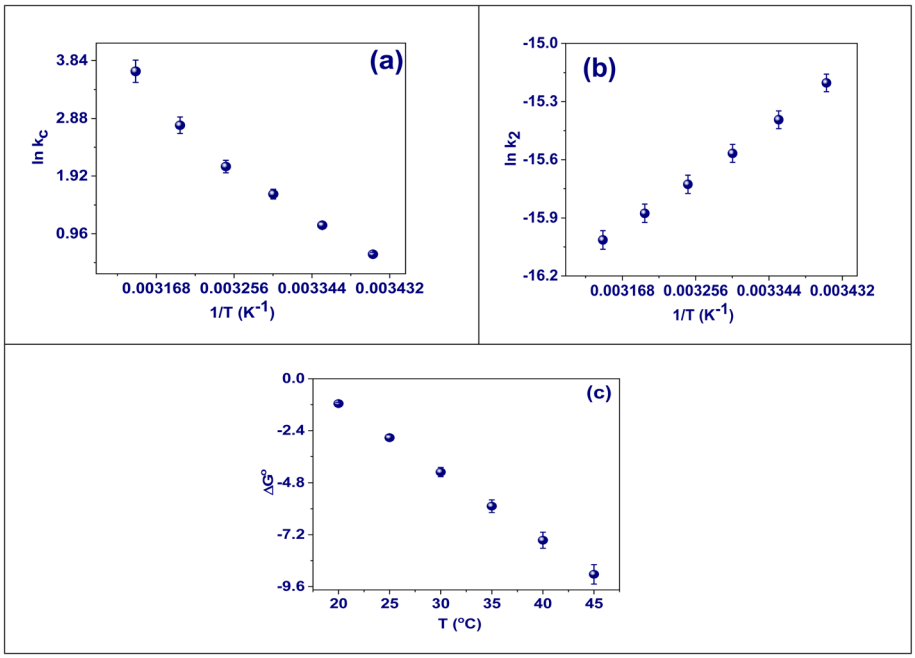

Fig. 8 Plots of the (a) van't Hoff model and (b) Arrhenius model. (c) Effect of temperature on Δ*G*° for adsorptionn of CIP onto PMCC composite sponge.

and grows better at higher temperatures is supported by Fig. 8(c), which shows that the Gibbs free energy (Δ*G*°) gets increasingly negative as the temperature rises. These observations are validated by the data presented in Table S12, where Δ*G*° declines from −1.15 kJ mol^{-1} at 293 K to −9.03 kJ mol^{-1} at 318 K. Additionally, the positive values of Δ*H*° (91.2 kJ mol^{-1}) and Δ*S*° (315.2 J mol^{-1} K^{-1}) reinforce the conclusions regarding the endothermic and entropy-driven dynamics of the process.[51] The thermodynamic assessment indicated a positive enthalpy change (Δ*H*° = 91.2 kJ mol^{-1}), much higher than the typical physisorption values below 40 kJ mol^{-1}, suggesting that ciprofloxacin adsorption onto the PMCC is mostly chemisorptive. This conclusion is corroborated by the Dubinin–Radushkevich (D–R) isotherm, which reveals a mean adsorption energy (*E* = 33.6 kJ mol^{-1}) that is indicative of chemical adsorption. Strong inner-sphere coordination likely occurs between the carbonyl and carboxylate groups of ciprofloxacin and the Lewis-acidic Pd^{2+} centers in the MOF. Additionally, hydrogen bonding and π–π stacking from the CS–CMC matrix and MOF ligands enhance these interactions. The high Δ*H*° suggests multilayer or cooperative interactions, where the first layer of chemisorbed species promotes further adsorption through mechanisms like hydrogen bonding, indicating a synergistic adsorption mechanism with strong coordination and non-covalent forces, aligning with the PMCC structural data. In summary, the thermodynamic analysis firmly establishes that the adsorption of CIP onto PMCC is a spontaneous, endothermic process characterized by improved randomness at the solid–liquid interface, with enhanced adsorption capacity and rate at elevated temperatures, thereby representing the efficacy of the PMCC under thermal conditions.[52]

3.7. Mechanism of interaction

The adsorption process of CIP onto the PMCC involves a series of synergistic interactions attributable to both the Pd-MOF and the chitosan–CMC biopolymeric matrix. A predominant driving force of this mechanism is electrostatic attraction, which is influenced by the pH of the solution. In this context, the zwitterionic, cationic, or anionic forms of CIP engage with the protonated $-NH_3^+$ groups of chitosan or the deprotonated $-COO^-$ groups of CMC. Additionally, hydrogen bonding plays a noteworthy role in stabilizing the adsorption, as the hydroxyl, amino, and carboxyl functional groups existing in the CS–CMC matrix, along with the oxygenated sites within the MOF, establish strong hydrogen bonds with the –COOH, –C═O, –NH, and F-containing groups of CIP. Furthermore, π–π stacking connections between the aromatic quinolone ring of CIP and the conjugated benzene linkers of the Pd-MOF serve to enhance the binding affinity. A critical mechanism at play is metal–ligand coordination, wherein the electron-donating carbonyl and carboxylate groups of CIP coordinate with the Lewis-acidic Pd^{2+} centers, resulting in the formation of robust inner-sphere complexes. These chemical interactions are augmented by van der Waals forces, hydrophobic interactions between the nonpolar regions of CIP and the polymeric network, and the physical filling of pores within the interconnected sponge-like architecture. The multi-interaction mechanism is further corroborated by FTIR and XPS analyses: the CIP-loaded PMCC shows significant FTIR shifts in the C═O region (1710–1620 cm^{-1}) and an expansion in the O–H/N–H band (3200–3400 cm^{-1}), indicative of hydrogen bonding and coordination effects. XPS data also confirm the presence of chemical binding, evidenced by an increased contribution of C–O/Pd–O in the O 1s spectrum, a shift towards higher binding energies in the N 1s

region due to electron donation during coordination, and a slight positive shift (<0.4 eV) in the Pd 3d spectrum, which substantiates the interaction between CIP's oxygen donors and the Pd centers (Fig. S2). In summary, the synergy among these forces, including electrostatic attraction, hydrogen bonding, π–π stacking, metal composite coordination, hydrophobic interactions, and pore entrapment, creates a comprehensive and effective adsorption mechanism that significantly enhances the CIP uptake and elucidates the high performance of the PMCC.[53]

3.8. Effect of salinity

Fig. 9 illustrates that the CIP removal efficiency by the PMCC demonstrates a marginal decline as the ionic strength increases. Specifically, as the ionic strength, indicated by NaCl concentration, escalates from 10 to 40 g L^{-1} at a pH of 8, there is an obvious reduction in the adsorption capability for CIP elimination. At salt concentrations of 10 to 40 g L^{-1}, sodium chloride (NaCl) was utilized as the ionic source to investigate how ionic strength influences the adsorption of CIP onto the PMCC. The Na^+ ions appeared to hinder the adsorption of CIP onto the sponge, as shown in Fig. 9. The competition among CIP and Na^+ ions for the active adsorption sites is responsible for this phenomenon, since it reduced their adsorption capacity, thus limiting their electrostatic connections. In this pH context, the cationic forms of CIP may experience either electrostatic competition or repulsion with Na^+ ions when present at lower concentrations, further diminishing the adsorption levels.[54] Moreover, the activity coefficients of CIP are influenced, leading to a deceleration of the sorption process. Furthermore, as ionic strength increases, the tendency for aggregation also rises, adversely affecting the electrostatic interactions involved in the sorption process.

3.9. Effect on actual water examples

Ciprofloxacin (CIP) elimination from distilled water, tap water, lake water, and wastewater from industries was evaluated as part of the study. In the experiments, these water samples were intentionally contaminated with 200 mg L^{-1} of CIP, using an adsorbent quantity of 0.02 g and a sample volume of 25 mL, with an interaction time of 100 min and a pH level of 8. The research also investigated the potential use of PMCC for water-treatment applications.[55] Despite the decline in the CIP removal efficiency from 96.7% in distilled water to 92.4% in tap water, 84.6% in lake water, and 72.66% in industrial wastewater, the removal rates remained sufficiently high, indicating the effectiveness of the method. These reductions in efficiency among different water types are not unexpected, due to the presence of numerous non-target positive ions that compete with CIP for the limited active adsorption sites on the adsorbent, thereby decreasing the general removal efficiency. Additionally, the relatively high efficiency of CIP removal using the PMCC in both industrial wastewater and lake water illustrates its significant potential for practical applications in wastewater treatment (Fig. 10).

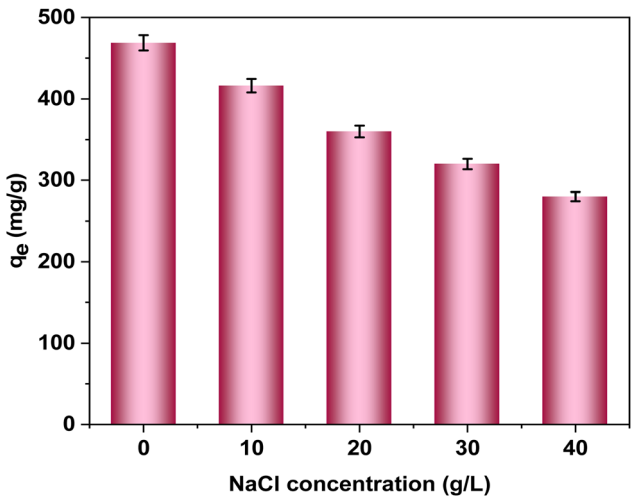

Fig. 9 Effect of salinity on the adsorption of CIP using PMCC.

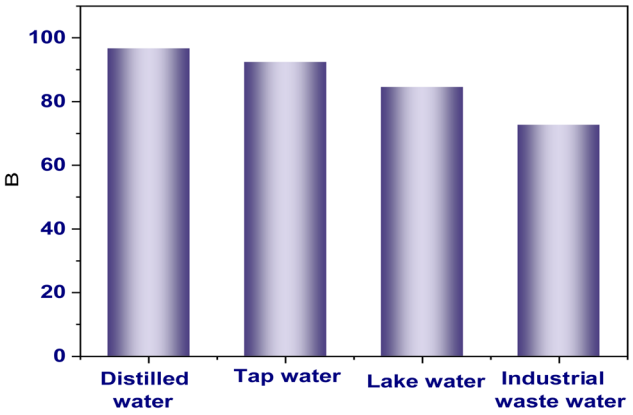

Fig. 10 Removal efficiency for CIP from different real water samples *via* PMCC.

3.10. Reusability

This study involved adding 0.02 g of PMCC to a 50 mL water solution containing 100 mg L^{-1} of CIP. The testing procedures were maintained at a constant pH of 8 for 100 min in order to enhance the adsorption efficacy of CIP. Following the filtration procedure, a 50 mL elution solution consisting of ethanol and 0.1 N HCl combined in a 7 : 3 volume ratio was applied to the CIP-saturated adsorbent to facilitate the elution of CIP. To enhance the interaction between the adsorbent and elution solvent, the adsorbent was continuously stirred for 1 hour at 25 °C. The PMCC was then extracted from the resultant mixture using centrifugation.[56] The material was cleaned with distilled water and then dried at 65 °C.[57] A significant decrease in retention capacities was observed during the course of five consecutive adsorption–desorption cycles; the values recorded at 97.5%, 95.4%, 93.6%, 87.4%, and 83.3% of the starting capacity, respectively, showed a steady fall. This decrease in uptake can be explained by the depletion of the active sites and changes in the material's particular geometric configuration, which worsened with each cycle. According to the findings, there are many opportunities for successful recycling

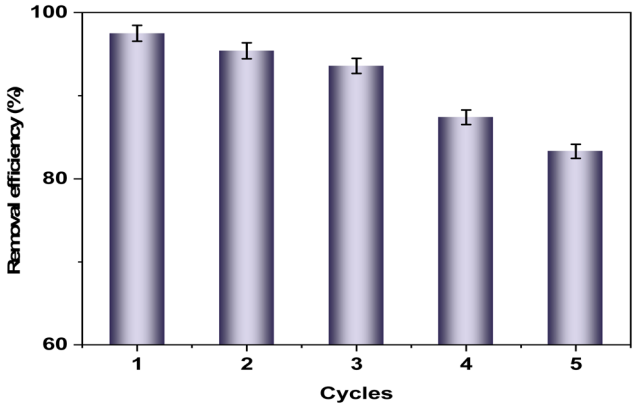

Fig. 11 Reusability of PMCC.

applications using the PMCC. As exposed in Fig. S3(a), XRD analysis was used to assess the structural stability of the PMCC following the regeneration procedure. The findings show that even after five regeneration cycles, the adsorbent's structural integrity was maintained. The PMCC performs consistently for up to five cycles, as shown in Fig. 11. This outcome demonstrates that the stability of the adsorbent is effectively maintained during the testing phase.[58,59] The FT-IR spectrum of the regenerated PMCC indicates that the composite retains structural integrity during regeneration, with only minor spectral shifts and intensity changes observed, reflecting the reversible adsorption–desorption process.[60] The wide absorption band in the 3400–3200 cm^{-1} range, attributed to the O–H and N–H stretching in chitosan, CMC, and hydroxyls in the Pd-MOF, shows a slight intensity decrease for the regenerated PMCC, suggesting some hydrogen-bond disruption. Aliphatic C–H stretching at 2920–2850 cm^{-1} remains stable, indicating the polymer backbone's integrity. In the fingerprint region, the band at 1650–1600 cm^{-1} for amide I and carboxylate modes indicates the reversible interactions with CIP, while the peak at 1570–1500 cm^{-1} decreases in intensity, reflecting CIP desorption. The strong C–O–C and C–O stretching bands in the 1100–1000 cm^{-1} range remain consistent, showing the polysaccharide network's stability.[61] Overall, despite minor changes, primary functional groups persist, demonstrating PMCC's chemical stability and structural resilience after regeneration (Fig. S3(b)).

3.11. Comparing other adsorbents

A thorough relative study of the different adsorbents used for CIP extraction is carried out using the data in Table S13. Importantly, the PMCC developed in this work has a noticeably higher adsorption capacity.[62,63] This exceptional efficacy highlights the PMCC's greater affinity for fluoroquinolone antibiotics, indicating its significant potential as a viable and efficient adsorbent for treating polluted water bodies.[64]

3.12. Statistical analysis

3.12.1. ANOVA. A thorough statistical examination of the model used to improve the adsorption and removal of CIP *via* the PMCC is provided by the ANOVA results. The model's strong prediction powers and statistical reliability are supported by this investigation. Interestingly, the model shows a highly significant *F*-value of 47.62, accompanied by a *P*-value below 0.0001, indicating that the parameters in question together significantly affect the CIP adsorption.[65] The coefficient of determination ($R^2 = 0.9839$) indicates that an impressive 98.39% of the inconsistency in the answer can be attributed to the proposed model. Furthermore, the adjusted R^2 value of 0.9633 reinforces the robustness of this model by taking into consideration the number of predictors involved. The predicted R^2, which stands at 0.7429, demonstrates a satisfactory level of predictive accuracy.[66] The analysis identifies several critical factors with significant contributions to the procedure: pH (*A*), time (*B*), and dose (*C*), among which time applies the greatest substantial effect ($F = 313.15$, $P < 0.0001$). The presence of significant quadratic terms (A^2, B^2, and C^2) suggests that these variables exhibit nonlinear dynamics. In terms of interaction effects, only the connection between time and dose (*BC*) exhibits statistical meaning ($P = 0.0129$), whereas the connections between pH and time (*AB*) and pH and dose (*AC*) do not reflect statistical significance. The presence of a nonsignificant lack of fit, accompanied by a substantial adequate precision value of 23.76, indicates a strong model fit and an effective signal-to-noise ratio.[67] Further validation of the thermodynamic model quality is indicated by additional metrics: a low standard deviation of 25.10; a coefficient of variation (CV) of 11%; and favorable values for the Prediction Sum of Squares (PRESS), Akaike Information Criterion corrected (AICc), and Bayesian Information Criterion (BIC). Taken together, this analytical assessment verifies that the performance of the PMCC sponge is notably affected by the variables under investigation, confirming the model's robustness and its appropriateness for optimizing the elimination of CIP from aqueous environments, as illustrated in Table 1.

Table S14 compares the modeling methods: linear, two-Factor Interaction (2FI), and quadratic models, for studying the CIP adsorption and elimination on PMCC, focusing on the sum of squared differences. The quadratic model proves to be the most suitable due to its better statistical performance.[68] The linear model has a significant *p*-value of 0.0001 but lower adjusted R^2 (0.7427) and predicted R^2 (0.6412), indicating moderate explanatory power. The 2FI model performs worse, with a predicted R^2 of 0.4209 and a non-significant *p*-value of 0.6208, showing that interaction effects do not sufficiently explain the CIP adsorption process. In contrast, the quadratic model excels with an adjusted R^2 of 0.9633 and a predicted R^2 of 0.7429, indicating an excellent fit and a low prediction error.[69] The statistical significance of the quadratic model ($p = 0.0005$) confirms its reliability in modeling primary effects and the curvature of the response surface. It is regarded as the best model for optimizing CIP removal on the PMCC sponge in experimental and practical contexts, as shown in Table S14.

3.12.2. Adequacy validation of the model. Fig. 12(a) shows a normal probability plot of superficially studentized residuals, essential for evaluating the statistical model of CIP adsorption and removal by PMCC. The residuals are compared to

Table 1 Examination of variance for the model's suitability

Source	Sum of squares	df	Mean squares	*F*-value	*P*-value	
Model	2.699×10^5	9	29 993.87	47.62	<0.0001	Significant
A-pH	3851.98	1	3851.98	6.12	0.0426	
B-time	1.972×10^5	1	1.972×10^5	313.15	<0.0001	
C-dose	15 920.05	1	15 920.05	25.28	0.0015	
AB	1448.76	1	1448.76	2.30	0.1731	
AC	573.69	1	573.69	0.9109	0.3717	
BC	6911.47	1	6911.47	10.97	0.0129	
A^2	14 273.57	1	14 273.57	22.66	0.0021	
B^2	26 971.88	1	26 971.88	42.83	0.0003	
C^2	69.53	1	69.53	0.1104	0.7494	
Residual	4408.65	7	629.81			
Lack of fit	4408.65	3	1469.55			
Pure error	0.0000	4	0.0000			
Cor. total	2.744×10^5	16				
Std. dev.	25.10					
Mean	228.15					
CV %	11.00					
R^2	0.9839					
Adjusted R^2	0.9633					
Predicted R^2	0.7429					
Adeq. precision	23.7573					
PRESS	70 538.35					
−2 log likelihood	142.73					
BIC	171.06					
AICc	199.40					

a theoretical standard distribution. Most points near the red diagonal line indicate minimal divergence, suggesting a roughly normal distribution and confirming ANOVA assumptions, thus enhancing the model's validity and reliability.[70] The lack of extreme outliers or non-linearity suggests no significant biases or unexplained patterns in the model. This supports the idea that the chosen quadratic model fits the data well and is effective for forecasting CIP adsorption behavior with the PMCC under the given experimental conditions.

Fig. 12(b) shows a predicted *vs.* actual plot, crucial for assessing the regression model's precision in forecasting CIP adsorption and removal on PMCC. Each orange square represents the predicted and actual experimental values. The diagonal line signifies perfect alignment; data points near this line indicate a strong correlation and high accuracy of the model.[71] No significant deviations or trends were observed, indicating that the model makes reliable predictions without major underestimations or overestimations across the response range. While some variation occurs at lower concentrations, the overall correlation supports the model's predictive reliability. High R^2 values and low residual error metrics from ANOVA confirm the effectiveness of the quadratic regression model for modeling CIP adsorption onto PMCC sponges under various conditions.

Fig. 12(c) shows a Box–Cox plot for control transformations to determine if a response variable transformation is needed for ANOVA or regression analysis in CIP adsorption and removal with the PMCC. The transformation limit, lambda (λ), is displayed on the horizontal axis, while the natural logarithm of residual sum of squares (ln(residual SS)) is represented on the vertical axis. The goal is to find the λ value that minimizes the residual totality of squares, indicated by the curve's lowest point, which is near $\lambda = 1$, marked by a green line within the 95% assurance interval shown by red and blue lines.[72] This indicates that a transformation is unnecessary, as the model aligns with the original data scale. A λ value near 1 suggests adherence to normality and constant variance, supporting the integrity of the numerical analysis without modifying the response variable. Thus, the Box–Cox plot confirms that the current model framework for CIP adsorption is suitable, with no need for transformation to improve fit or stabilize variance.[73,74]

Fig. 12(d) shows a residuals *vs.* predicted plot to assess the adequacy of the regression model for CIP adsorption and removal by PMCC. The externally studentized residuals, standardized to account for data influence, are on the vertical axis, while the predicted values are on the horizontal axis. Ideally, residuals should be randomly distributed around zero, indicating homoscedasticity and an unbiased model.[75] In this plot, the residuals are uniformly distributed around the zero line, mostly within the control limits ($\pm$4.81963) and without outliers. This suggests no significant violations of model assumptions. The lack of curvature in the residuals supports the linearity assumption and indicates stable variance across predictions. Overall, these insights affirm the strength of the regression model, likely quadratic, in accurately modeling the adsorption of CIP on PMCC without needing further adjustments.[76–78]

Fig. 12(e) displays a perturbation plot assessing the sensitivity of CIP adsorption capacity (q_e) to variations in a single factor while others remain constant. It highlights the effects of pH (*A*), contact time (*B*), and adsorbent amount (*C*) on CIP adsorption onto PMCC. Factor *B* (contact time) shows the most curvature, indicating a strong impact on the adsorption

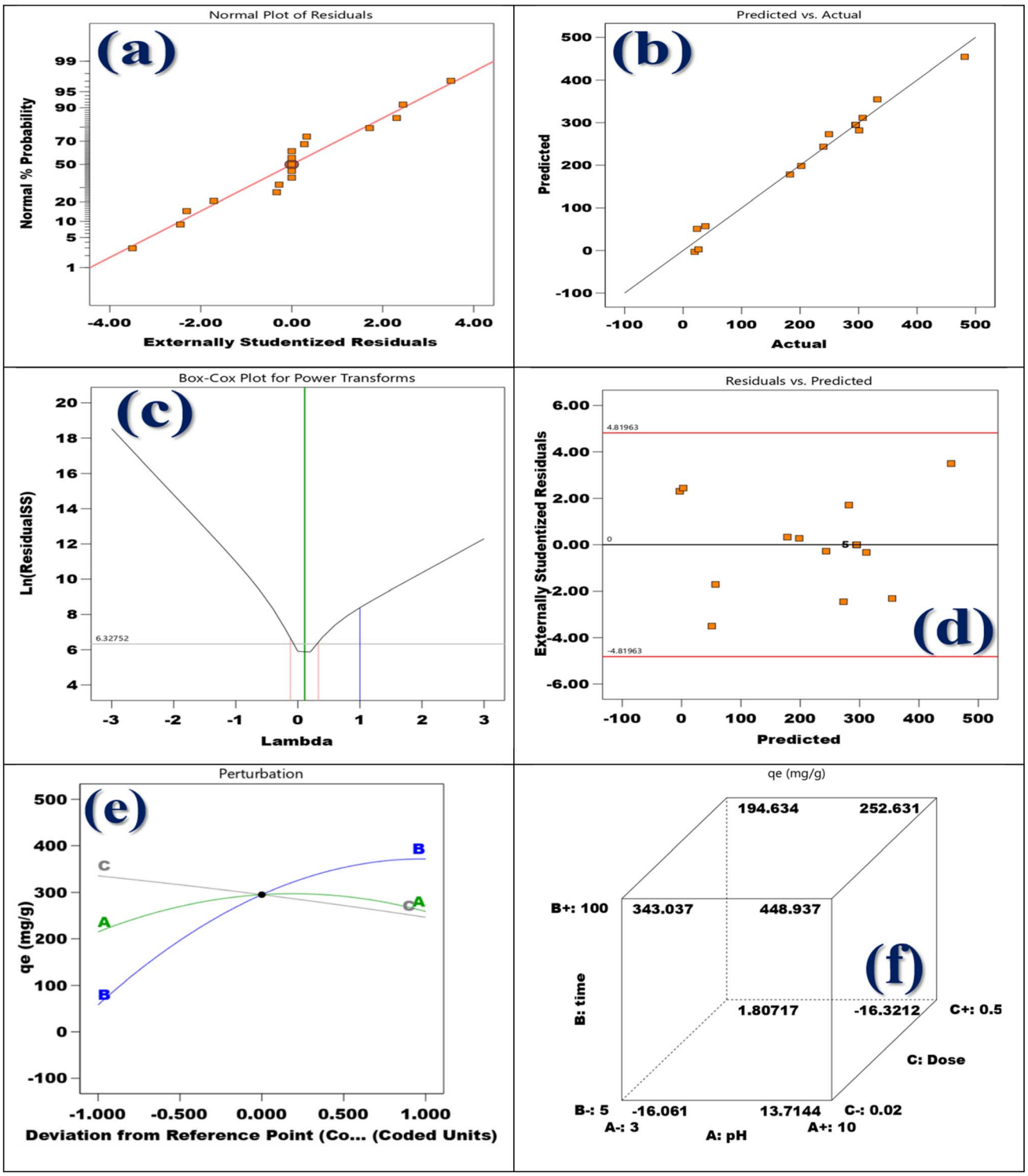

Fig. 12 (a) Normal probability plot of superficially studentized residuals, (b) predicted *vs.* actual plot for assessing the regression model's precision, (c) Box–Cox plot, (d) residuals *vs.* predicted plot to assess the adequacy of the regression model, and (e) perturbation and (f) cube plots.

capacity. As contact time increases from −1 to +1, q_e sharply rises to over 400 mg g^{-1}, reflecting a significant positive influence. In comparison, factor *A* (pH) exhibits a moderate effect with a nonlinear curve, while factor *C* (dose) shows minimal variations in CIP uptake with changes in the adsorbent dose. The plot identifies key variables for optimization, emphasizing the importance of contact time in enhancing CIP removal.[79] This visual confirms the ANOVA and regression findings, indicating that contact time is vital for improving the PMCC sponge's adsorption efficiency.

Fig. 12(f) shows a cube plot that exemplifies how three factors, *i.e.*, pH (*A*), interaction time (*B*), and adsorbent dose (*C*),

influence the adsorption capacity (q_e) of CIP on PMCC. Each corner of the cube corresponds to unique combinations of low (−) and high (+) factor levels, showing respective adsorption capacities in mg g^{-1}. The maximum adsorption (q_e = 448.937 mg g^{-1}) happens at pH 10, for the 100-min interaction and 0.5 g adsorbent dose case, indicating strong synergies among these factors for improved CIP removal. In contrast, lower q_e values occur with minimized factors, particularly at the 5-min contact time, leading to significantly reduced adsorption (*e.g.*, q_e = −16.061 mg g^{-1} at pH 3 and 0.02 g).[80–82] The plot validates the ANOVA and perturbation analysis, emphasizing interaction time as the primary variable affecting adsorption, followed by pH and then dose. This visual tool assists in pinpointing the optimal parameter combinations and extreme cases, offering vital insights for establishing operational protocols in water treatment utilizing PMCC.[83]

3.12.3. Model experimental designs and response surface analysis. Fig. 13(a) shows a 3D surface design, 2D contour design, and desirability design illustrating the effects of the adsorbent amount (*A*) and communication time (*B*) on the ciprofloxacin (CIP) adsorption capacity (q_e) on the PMCC sponge. The 3D surface design reveals that increases in both the adsorbent amount and interaction time improved the CIP adsorption significantly, with q_e values from 19.7 mg g^{-1} to 481.4 mg g^{-1}. The influence of contact time is notably stronger, as indicated by a steeper gradient, while higher doses result in a flattening surface, suggesting diminishing returns. The 2D contour design confirms that at lower doses and contact times, q_e varies greatly, whereas at higher levels, it shows a plateau. The desirability plot indicates that optimal conditions for CIP removal occur when the contact time is over 80 min and the adsorbent dose is above 0.35 g, achieving maximum desirability scores above 0.8.[84] This detailed analysis illustrates that while both factors enhance the CIP removal efficiency, the contact time is the most pivotal factor, and optimizing both parameters is essential for maximizing the efficacy of the PMCC in water-treatment processes.[85]

Fig. 13(b) presents three visual plot illustrations: 3D surface, 2D contour, and desirability, showing the influence of the pH level (*A*) and adsorbent amount (*B*) on the adsorption capacity

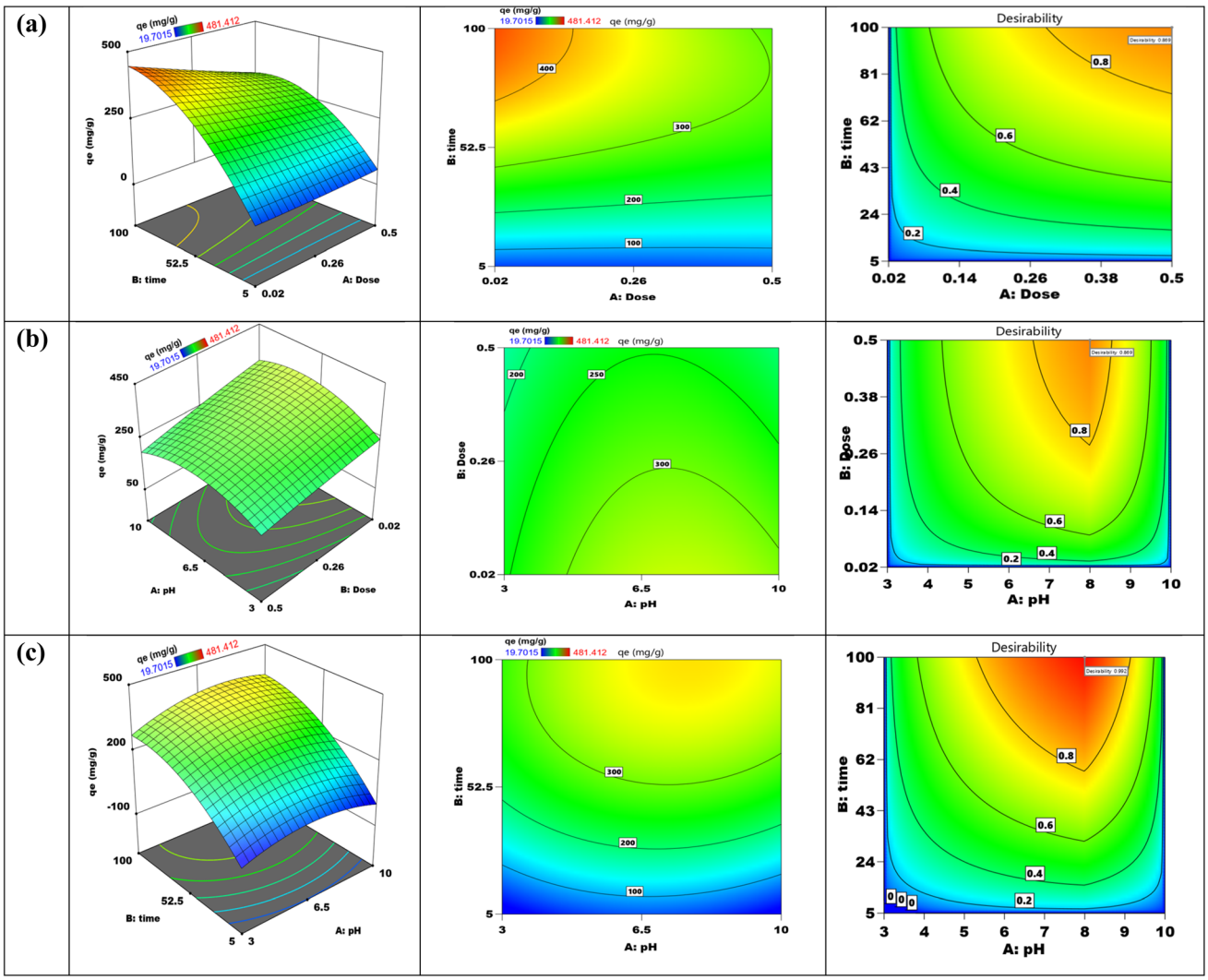

Fig. 13 3D interaction, contour, and desirability plots as the interaction between (a) dose and time, (b) dose and pH, and (c) pH and time.

(q_e) and overall process desirability for CIP elimination using PMCC. The 3D surface plot indicates that both variables positively influence q_e, peaking at about 481.4 mg g^{-1}, particularly at higher pH levels and moderate-to-high adsorbent doses. The curvature reveals the pH's stronger influence compared to the dose, leading to significant adsorption efficiency improvements from acidic to nearly neutral pH, stabilizing under alkaline conditions. The 2D contour plot supports this, showing enhanced q_e zones as pH shifts from 3 to 10, with less impact from the dose. The desirability plot indicates that the optimal conditions for achieving desirability over 0.8 occur around pH 8 to 9, with adsorbent doses being above 0.35 g, reflecting the best scenario for maximizing the CIP removal. These visualizations highlight the pH's crucial role in boosting the adsorption efficiency, with dosage being moderately significant, aiding in defining ideal operational parameters for effective PMCC water treatment.[86]

Fig. 13(c) illustrates three plot analyses: 3D surface, 2D contour, and desirability, showing the influence of pH (A) and contact time (B) on the adsorption capacity (q_e) of CIP on PMCC. The 3D plot indicates that increasing both pH and contact time enhances the adsorption capacity, peaking around 481.4 mg g^{-1} under alkaline conditions and with extended durations.[87] The surface curvature indicates high sensitivity to pH, showing that the sponge's effectiveness increases as the conditions shift from acidic to neutral to basic. This enhancement likely results from the changes in surface charge and better interactions with the CIP molecules. The 2D contour plot illustrates rising q_e values,

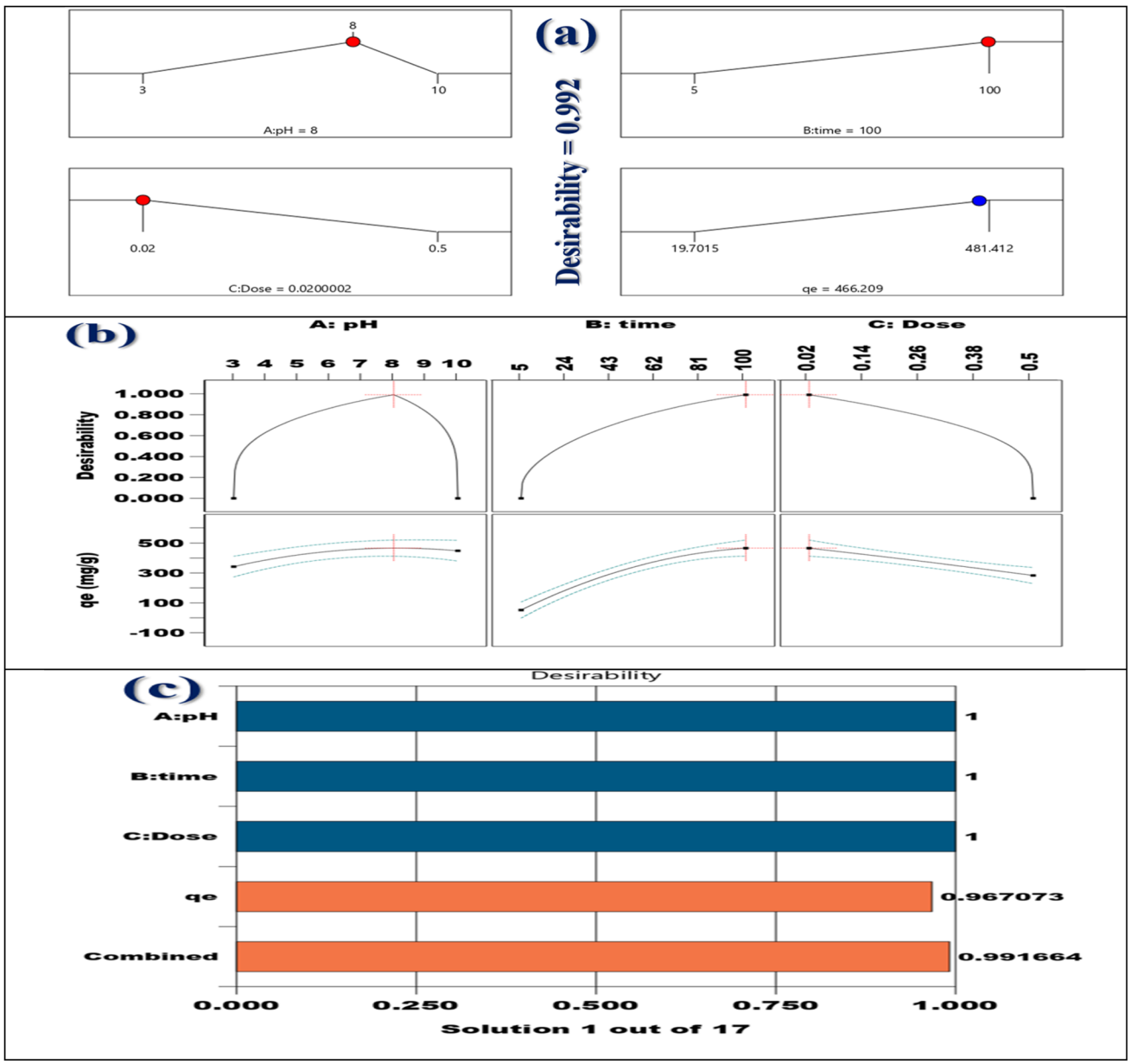

Fig. 14 (a) Numerical optimization using desirability function analysis, (b) Box–Behnken RSM desirability and main-effect profiles for adsorption optimization, and (c) a bar graph of individual desirability.

with a notable shift from low pH and short contact times to high pH and extended contact times. After 50 min, the contact time has a stronger impact. The desirability plot reveals optimal conditions, with values over 0.8 occurring when the pH is above 8 and the contact time exceeds 80 minutes. These findings confirm that alkaline pH and longer contact time meaningfully enhance the PMCC sponge's adsorption, highlighting its potential for effective wastewater treatment.

3.12.4. The model validation process and the desirability method. Fig. 14(a) shows the optimization graph for CIP adsorption onto PMCC, emphasizing the optimal operational parameters for maximizing the adsorption capacity (q_e), with a desirability score of 0.992. Individual factor plots illustrate the contributions of pH, interaction time, and adsorbent amount to this optimal result.[88] The ideal pH is 8, maximizing adsorption efficiency due to favorable electrostatic interactions. The contact time of 100 min, the longest tested, shows that extended exposure improves adsorption. The adsorbent dose can be minimized to 0.02 g, indicating that even small amounts of PMCC are effective under these conditions. The adsorption capacity achieved is $q_e = 466.209$ mg g^{-1}, close to the system's maximum of 481.412 mg g^{-1}. This demonstrates that a high adsorption efficiency can be reached with minimal material input when the pH and contact time are optimized, making it effective for water-treatment applications.

Fig. 14(b) shows a profile for predicting the desirability and response regarding CIP adsorption on PMCC. It highlights ideal ranges for pH (A), interaction time (B), and adsorbent amount (C), vital for improving the process desirability and adsorption capacity (q_e). The curves indicate that optimal adsorption occurs at pH 8, 100 min interaction time, and 0.02 g adsorbent dose, reaching a desirability peak of about 1.0.[89] Effective CIP removal is maximized under mildly alkaline conditions, with a longer exposure period and minimal adsorbent use, optimizing performance while reducing material consumption. Response curves for q_e show that adsorption capacity increases with pH and time, nearing 500 mg g^{-1}. The dose–response curve peaks at the lowest tested dose (0.02 g) before decreasing or leveling off at higher doses. This suggests that beyond an optimal pH and time, increasing the adsorbent dose does not significantly enhance performance and may reduce efficiency due to site saturation or clustering. Overall, these results indicate that the PMCC sponge functions best at low dosages, extended duration, and slightly alkaline pH, promoting resource-efficient water treatment.

Fig. 14(c) presents a desirability bar chart summarizing the optimal conditions for CIP adsorption onto PMCC, derived from one of the optimal solutions out of the 17 optimization runs. The chart shows individual desirability scores for pH (A), interaction time (B), and adsorbent dose (C), alongside the output response adsorption capacity (q_e) and the overall combined desirability. Each input variable achieves a perfect score of 1.0, indicating precise alignment with the optimal targets. The desirability for q_e is 0.9671, indicating that the adsorption performance is close to the maximum (near 481.4 mg g^{-1}). The combined desirability score is 0.9917, confirming that the optimized conditions effectively balance all parameters to maximize CIP removal using the PMCC sponge, emphasizing both efficiency and practicality.[90]

4. Conclusion

This study demonstrates the successful growth of a new bio-derived composite sponge known as PMCC, which is created by joining Pd-MOFs within a matrix made of chitosan and carboxymethyl cellulose. The PMCC exhibited impressive capabilities in adsorbing ciprofloxacin (CIP) from water sources. Detailed physicochemical analysis confirmed its structural stability and porous characteristics, as well as the functional groups that facilitate CIP adsorption. The results of batch adsorption experiments highlighted the significance of aspects like pH, interaction time, amount, and temperature on the adsorption technique. The adsorption behavior was affiliated with the Langmuir isotherm model, achieving a maximum capacity of 480.5 mg g^{-1}, while the kinetic studies indicated that the pseudo-second-order model best fit the data, suggesting a chemisorption mechanism. Thermodynamic investigation exposed that the process is spontaneous, as well as endothermic, with ΔH° of 91.2 kJ mol^{-1} and ΔS° of 315.2 J mol^{-1} K^{-1}. The mechanism of CIP removal was found to involve hydrogen bonding, electrostatic forces, and π–π interactions. Furthermore, the PMCC demonstrated commendable reusability, maintaining a high level of adsorption efficiency even after five successive regeneration cycles. Optimization through Box–Behnken design reaffirmed the sponge's effectiveness under ideal conditions. In summary, the PMCC is highlighted as a maintainable, efficient, and reusable solution for the removal of medicinal pollutants from aquatic environments.

Conflicts of interest

The authors affirm that none of the work described in this publication may have been influenced by any known competing financial interests or personal relationships.

Data availability

The data that support the findings of this study are available from the corresponding author upon reasonable request.

Supplementary information (SI) is available. See DOI: https://doi.org/10.1039/d5ra08409a.

Acknowledgements

This work was supported and funded by the Deanship of Scientific Research at Imam Mohammad Ibn Saud Islamic University (IMSIU) (grant number IMSIU-DDRSP2602).

References

1 M. Abbas, S. Kaddour and M. Trari, Kinetic and equilibrium studies of cobalt adsorption on apricot stone activated carbon, *J. Ind. Eng. Chem.*, 2014, **20**, 745–751.

2 A. Ahmadpour, M. Tahmasbi, T. R. Bastami and J. A. Besharati, Rapid removal of cobalt ion from aqueous solutions by almond green hull, *J. Hazard. Mater.*, 2009, **166**, 925–930.

3 D. N. Ahmed, L. A. Naji, A. A. Faisal, N. Al-Ansari and M. Naushad, Waste foundry sand/MgFe-layered double hydroxides composite material for efficient removal of Congo red dye from aqueous solution, *Sci. Rep.*, 2020, **10**, 2042.

4 P. A. Alaba, N. A. Oladoja, Y. M. Sani, O. B. Ayodele, I. Y. Mohammed, S. F. Olupinla and W. M. W. Daud, Insight into wastewater decontamination using polymeric adsorbents, *J. Environ. Chem. Eng.*, 2018, **6**, 1651–1672.

5 O. Alagha, M. S. Manzar, M. Zubair, I. Anil, N. D. Mu'azu and A. Qureshi, Magnetic Mg-Fe/LDH intercalated activated carbon composites for nitrate and phosphate removal from wastewater: Insight into behavior and mechanisms, *Nanomaterials*, 2020, **10**, 1361.

6 T. Anirudhan, F. Shainy and J. Deepa, Effective removal of Cobalt (II) ions from aqueous solutions and nuclear industry wastewater using sulfhydryl and carboxyl functionalised magnetite nanocellulose composite: batch adsorption studies, *Chem. Ecol.*, 2019, **35**, 235–255.

7 S. Babić, A. Zelenika, J. Macan and M. Kaštelan-Macan, Ultrasonic extraction and TLC determination of glyphosate in the spiked red soils, *Agric. Conspectus Sci.*, 2005, **70**, 99–103.

8 Y. Bai, Z. Wu and X. Cheng, Dual-functional nanofiber membranes for simultaneous removal of heavy metals and organic pollutants, *Environ. Pollut.*, 2023, **315**, 120341.

9 D. Cai, Y. Zhang, J. Li, D. Hu, M. Wang, G. Zhang and J. Yuan, Intermolecular interactions in mixed dye systems and the effects on dye wastewater treatment processes, *RSC Adv.*, 2024, **14**, 373–381.

10 B. Chen, J. Wang and Z. Gao, Synergistic enhancement in bimetallic MOF adsorbents for heavy metal remediation, *Environ. Sci.: Nano*, 2023, **10**, 998–1010.

11 W. Cheng, Y. Liu and H. Zhang, Engineering nanofiber composites for water decontamination, *Chem. Eng. J. Adv.*, 2023, **13**, 100394.

12 R. Sanjay, S. Tejeshwini, K. Mamatha and S. Dinesh, Comparative study on structural evaluation of flexible pavement using BBD and FWD, *Mater. Today: Proc.*, 2022, **60**, 608–615.

13 R. Wu, A. S. Abdulhameed, A. H. Jawad, S. K. Yong, H. Li, Z. A. ALOthman, L. D. Wilson and S. Algburi, Development of a chitosan/nanosilica biocomposite with arene functionalization via hydrothermal synthesis for acid red 88 dye removal, *Int. J. Biol. Macromol.*, 2023, **252**, 126342.

14 A. Guesmi, N. B. Hamadi, W. A. El-Fattah, A. Subaihi, A. A. Alluhaybi, M. G. El-Desouky and A. A. El-Bindary, Efficient removal of ciprofloxacin in aqueous solutions by magnetic Se-MOF embedded within a biopolymer (chitosan/alginate): Adsorptive behavior, mechanism study, and optimization using Box-Behnken design, *Int. J. Biol. Macromol.*, 2025, **314**, 144274.

15 N. B. Hamadi, A. Guesmi, W. A. El-Fattah, T. A. Altalhi, M. A. El-Bindary, M. G. El-Desouky and A. A. El-Bindary, Sustainable removal of Cd(II) using β-Cyclodextrin/Polyethylenimine hydrogel beads embedded with silver-MOFs: Synthesis, characterization, mechanism, and process optimization, *Int. J. Biol. Macromol.*, 2025, **319**, 145663.

16 R. S. Dassanayake, S. Acharya and N. Abidi, Recent advances in biopolymer-based dye removal technologies, *Molecules*, 2021, **26**, 4697.

17 M. Dehghani, S. Nasseri and M. Karamimanesh, Removal of 2, 4-Dichlorophenolyxacetic acid (2, 4-D) herbicide in the aqueous phase using modified granular activated carbon, *J. Environ. Health Sci. Eng.*, 2014, **12**, 1–10.

18 S. Ghosh, S. Pourebrahimi, A. Malloum, O. J. Ajala, S. S. AlKafaas, H. Onyeaka, N. D. Nnaji, A. Oroke, C. Bornman and O. Christian, A review on ciprofloxacin removal from wastewater as a pharmaceutical contaminant: Covering adsorption to advanced oxidation processes to computational studies, *Mater. Today Commun.*, 2023, **37**, 107500.

19 M. H. Dehghani, K. Yetilmezsoy, M. Salari, Z. Heidarinejad, M. Yousefi and M. Sillanpää, Adsorptive removal of cobalt (II) from aqueous solutions using multi-walled carbon nanotubes and γ-alumina as novel adsorbents: Modelling and optimization based on response surface methodology and artificial neural network, *J. Mol. Liq.*, 2020, **299**, 112154.

20 E. Demirbaş, Adsorption of cobalt (II) ions from aqueous solution onto activated carbon prepared from hazelnut shells, *Adsorpt. Sci. Technol.*, 2003, **21**, 951–963.

21 A. H. Jawad, U. K. Sahu, N. A. Jani, Z. A. ALOthman and L. D. Wilson, Magnetic crosslinked chitosan-tripolyphosphate/MgO/Fe3O4 nanocomposite for reactive blue 19 dye removal: Optimization using desirability function approach, *J. Surf. Interfaces*, 2022, **28**, 101698.

22 A. S. Abdulhameed, A. H. Jawad, E. Kashi, K. A. Radzun, Z. A. ALOthman and L. D. Wilson, Insight into adsorption mechanism, modeling, and desirability function of crystal violet and methylene blue dyes by microalgae: Box-Behnken design application, *Algal Res.*, 2022, **67**, 102864.

23 A. H. Jawad, A. S. Abdulhameed, S. Surip and S. Sabar, Adsorptive performance of carbon modified chitosan biopolymer for cationic dye removal: kinetic, isotherm, thermodynamic, and mechanism study, *Int. J. Environ. Anal. Chem.*, 2022, **102**, 6189–6203.

24 G. H. Al-Hazmi, L. A. Albedair, A. M. Alsuhaibani, S. H. Alrefaee, I. Althagafi, Q. Mohsen, M. G. El-Desouky, A. A. El-Bindary and K. A. Asla, Synthesis and characterization of functionalized yttrium metal-organic frameworks encapsulated onto bi-polymers for effective removal of As(III); Adsorption isotherms, kinetic, and optimization via Box-Behnken design, *Mater. Today Commun.*, 2025, **45**, 112244.

25 E. Miguel-Casañ, M. D. Darawsheh, V. Fariña-Torres, I. J. Vitórica-Yrezábal, E. Andres-Garcia, M. Fañanás-Mastral and G. Mínguez Espallargas, Heterometallic palladium–iron metal–organic framework as a highly active

catalyst for cross-coupling reactions, *Chem. Sci.*, 2023, **14**, 179–185.
26 E. Díez, R. Miranda, J. M. López, A. Jiménez, N. Conte and A. Rodríguez, Adsorption of Cobalt onto Zeolitic and Carbonaceous Materials: A Review, *Separations*, 2024, **11**, 232.
27 D. Gago, R. Chagas, L. M. Ferreira, S. Velizarov and I. Coelhoso, A novel cellulose-based polymer for efficient removal of methylene blue, *Membranes*, 2020, **10**, 13.
28 M. Ghaedi, S. Hajati, F. Karimi, B. Barazesh and G. Ghezelbash, Equilibrium, kinetic and isotherm of some metal ion biosorption, *J. Ind. Eng. Chem.*, 2013, **19**, 987–992.
29 J. He, J. Xu and Y. Luo, Green synthesis of electrospun nanofiber composites for water purification, *ACS Sustain. Chem. Eng.*, 2023, **11**, 2476–2489.
30 A. R. Hernández-Martínez, G. A. Molina, L. F. Jiménez-Hernández, A. H. Oskam, G. Fonseca and M. Estevez, Evaluation of inulin replacing chitosan in a polyurethane/polysaccharide material for Pb2+ removal, *Molecules*, 2017, **22**, 2093.
31 J. Huang, Y. Liu and Y. Zhou, Comparative evaluation of treatment technologies for Cr(VI) removal: A critical review, *Environ. Technol. Rev.*, 2022, **11**, 1–25.
32 A. Hussein and M. Scholz, Treatment of artificial wastewater containing two azo textile dyes by vertical-flow constructed wetlands, *Environ. Sci. Pollut. Res.*, 2018, **25**, 6870–6889.
33 M. Imran Din, M. L. Mirza, S. Ata, M. Athar and I. U. Mohsin, Thermodynamics of biosorption for removal of Co (II) ions by an efficient and ecofriendly biosorbent (Saccharum bengalense): kinetics and isotherm modeling, *J. Chem.*, 2013, **2013**, 528542.
34 I. Ishraydeh, O. Hamed, A. Deghles, S. Jodeh, K. Azzaoui, A. Hasan, M. Assali, A. Jaseer, W. Mansour and G. G. Hacıosmanoğlu, Olive industry liquid waste from trash to metal adsorbent for wastewater purification, *BMC Chem.*, 2024, **18**, 4.
35 M. Jahangiri-Rad, K. Nadafi, A. Mesdaghinia, R. Nabizadeh, M. Younesian and M. Rafiee, Sequential study on reactive blue 29 dye removal from aqueous solution by peroxy acid and single wall carbon nanotubes: experiment and theory, *Iran. J. Environ. Health Sci. Eng.*, 2013, **10**, 1–8.
36 Y. Jiao, X. Liu and S. Wang, Effect of pH and temperature on Cr(VI) adsorption using composite membranes, *Environ. Sci. Pollut. Res.*, 2023, **30**, 8897–8910.
37 M. A. Khan, M. A. Rauf and P. Wang, Recent advancements in Cr(VI) adsorption using sustainable materials, *Chem. Eng. J.*, 2023, **452**, 139121.
38 A. Kumar, T. Das, R. S. Thakur, Z. Fatima, S. Prasad, N. G. Ansari and D. K. Patel, Synthesis of biomass-derived activated carbons and their immobilization on alginate gels for the simultaneous removal of Cr (VI), Cd (II), Pb (II), As (III), and Hg (II) from water, *ACS Omega*, 2022, **7**, 41997–42011.
39 A. Labena, A. E. Abdelhamid, A. S. Amin, S. Husien, L. Hamid, G. Safwat, A. Diab, A. A. Gobouri and E. Azab, Removal of methylene blue and congo red using adsorptive membrane impregnated with dried Ulva fasciata and Sargassum dentifolium, *Plants*, 2021, **10**, 384.
40 J. Y. Lee, H. J. Lee and K. Cho, Functional nanofiber composites for environmental remediation, *Adv. Funct. Mater.*, 2023, **33**, 2207365.
41 X. Liu, Y. Huang, S. Duan, Y. Wang, J. Li, Y. Chen, T. Hayat and X. Wang, Graphene oxides with different oxidation degrees for Co (II) ion pollution management, *Chem. Eng. J.*, 2016, **302**, 763–772.
42 I. Langmuir, The constitution and fundamental properties of solids and liquids. Part I. Solids, *J. Am. Chem. Soc.*, 1916, **38**, 2221–2295.
43 H. M. F. Freundlich, Over the adsorption in solution, *J. Phys. Chem.*, 1906, **57**, 385–471.
44 M. Dubinin, The equation of the characteristic curve of activated charcoal, *Proc. Acad. Sci. USSR, Phys. Chem. Sect.*, 1947, **55**, 327–329.
45 V. P. M. I. Tempkin, Kinetics of ammonia synthesis on promoted iron catalyst, *Acta Phys. Chim. USSR*, 1940, **12**, 327–356.
46 D. P. Vargas, L. Giraldo and J. C. Moreno-Piraján, CO2 adsorption on activated carbon honeycomb-monoliths: a comparison of Langmuir and Toth models, *Int. J. Mol. Sci.*, 2012, **13**, 8388–8397.
47 S. K. Lagergren, About the theory of so-called adsorption of soluble substances, *Sven. Vetensk. Akad. Handl.*, 1898, **24**, 1–39.
48 Y.-S. Ho and G. McKay, Sorption of dye from aqueous solution by peat, *Chem. Eng. J.*, 1998, **70**, 115–124.
49 W. J. Weber Jr and J. C. Morris, Kinetics of adsorption on carbon from solution, *J. Sanit. Eng. Div.*, 1963, **89**, 31–59.
50 M. H. Dehghani, A. Dehghan and A. Najafpoor, Removing Reactive Red 120 and 196 using chitosan/zeolite composite from aqueous solutions: Kinetics, isotherms, and process optimization, *J. Ind. Eng. Chem.*, 2017, **51**, 185–195.
51 E. C. Lima, A. Hosseini-Bandegharaei, J. C. Moreno-Piraján and I. Anastopoulos, A critical review of the estimation of the thermodynamic parameters on adsorption equilibria. Wrong use of equilibrium constant in the Van't Hoof equation for calculation of thermodynamic parameters of adsorption, *J. Mol. Liq.*, 2019, **273**, 425–434.
52 H. N. Tran, S.-J. You, A. Hosseini-Bandegharaei and H.-P. Chao, Mistakes and inconsistencies regarding adsorption of contaminants from aqueous solutions: a critical review, *Water Res.*, 2017, **120**, 88–116.
53 Y. Liu, Z. Sun and T. Zhang, Development of CS/PCL nanofiber membranes with enhanced mechanical and adsorption properties, *Carbohydr. Polym.*, 2022, **276**, 118778.
54 F. Maleki, M. Gholami, R. Torkaman, M. Torab-Mostaedi and M. Asadollahzadeh, Multivariate optimization of removing of cobalt (II) with an efficient aminated-GMA polypropylene adsorbent by induced-grafted polymerization under simultaneous gamma-ray irradiation, *Sci. Rep.*, 2021, **11**, 18317.
55 S. M. Mousavi, A. Ghasemi and M. Yari, Sustainable synthesis of CS/PCL nanocomposites for environmental applications, *Environ. Res.*, 2023, **219**, 115047.

56 H. Nadaroglu and E. Kalkan, Removal of cobalt (II) ions from aqueous solution by using alternative adsorbent industrial red mud waste material, *Int. J. Phys. Sci.*, 2012, **7**, 1386–1394.
57 C. Noè, M. Zanon, A. Arencibia, M.-J. López-Muñoz, N. Fernández de Paz, P. Calza and M. Sangermano, UV-cured chitosan and gelatin hydrogels for the removal of as (V) and Pb (II) from water, *Polymers*, 2022, **14**, 1268.
58 İ. Ömer, Ş. Taşar and N. Duranay, Removal of basic yellow dye molecules with chitosan-based magnetic field-sensitive particles from the aqueous solution, *Polymer*, 2024, 127895.
59 E. Murugan, J. N. Jebaranjitham, K. J. Raman, A. Mandal, D. Geethalakshmi, M. D. Kumar and A. Saravanakumar, Insoluble dendrimer-grafted poly (vinylimidazole) microbeads stabilized with mono/bimetallic nanoparticle catalysts for effective degradation of malachite green, *New J. Chem.*, 2017, **41**, 10860–10871.
60 K. M. Arumugam Poongan, A. Vinitha, G. Deenadayalan, A. Mandal, E. Murugan, Z. Khan and X. Jiang, Synthesis and characterization of new Copper-MOF grafted poly (n-butyl methacrylate-co-2-acryloyloxy ethyl trimethyl ammonium chloride) electrode for symmetric and asymmetric supercapacitor applications, *J. Indian Chem. Soc.*, 2025, **102**, 102229.
61 J. Guo, H. Ma, H. Shang, W. Wang, R. Yang, S. Wang, Y. Miao, D. L. Phillips, G. Li and S. Xiao, Dual-site Langmuir-Hinshelwood mechanism in ZnCr-LDH/NH2-UIO66 heterojunction for efficient photocatalytic NO oxidation, *J. Hazard. Mater.*, 2025, **492**, 138060.
62 W. Dai, C. Wang, Y. Wang, J. Sun, H. Ruan, Y. Xue and S. Xiao, Unlocking photocatalytic NO removal potential in an S-type UiO-66-NH2/ZnS (en) 0.5 heterostructure, *Interdiscip. Mater.*, 2024, **3**, 400–413.
63 M.-Y. Heng, H.-L. Shao, J.-T. Sun, Q. Huang, S.-L. Shen, G.-Z. Yang, Y.-H. Xue and S.-N. Xiao, Harnessing S-scheme junctions for enhanced CO2 photoreduction: molecular bonding of copper (II) complexes onto K-doped polymeric carbon nitride via microwave heating, *Rare Met.*, 2025, **44**, 1108–1121.
64 X. Pan, J. Wang and D. Zhang, Sorption of cobalt to bone char: Kinetics, competitive sorption and mechanism, *Desalination*, 2009, **249**, 609–614.
65 H. S. Kusuma, A. N. Amenaghawon, H. Darmokoesoemo, Y. A. Neolaka, B. A. Widyaningrum, S. U. Onowise and C. L. Anyalewechi, A comparative evaluation of statistical empirical and neural intelligence modeling of Manihot esculenta-derived leaves extract for optimized bio-coagulation-flocculation of turbid water, *Ind. Crops Prod.*, 2022, **186**, 115194.
66 H. Hadiyanto, M. Christwardana, W. Widayat, A. K. Jati and S. I. Laes, Optimization of flocculation efficiency and settling time using chitosan and eggshell as bio-flocculant in Chlorella pyrenoidosa harvesting process, *Environ. Technol. Innovation*, 2021, **24**, 101959.
67 H. S. Kusuma, R. G. M. Sudrajat, D. F. Susanto, S. Gala and M. Mahfud, Response surface methodology (RSM) modeling of microwave-assisted extraction of natural dye from Swietenia mahagony: A comparation between Box-Behnken and central composite design method, *AIP Conference Proceedings*, AIP Publishing, 2015.
68 A. H. Jawad and S. Surip, Upgrading low rank coal into mesoporous activated carbon via microwave process for methylene bluedye adsorption: Box Behnken Design and mechanism study, *Diamond Relat. Mater.*, 2022, **127**, 109199.
69 H. Kusuma, M. Syahputra, D. Parasandi, A. Altway and M. Mahfud, Optimization of microwave hydrodistillation of dried patchouli leaves by response surface methodology, *Rasayan J. Chem.*, 2017, **10**, 861–865.
70 A. H. Jawad, U. K. Sahu, M. S. Mastuli, Z. A. ALOthman and L. D. Wilson, Multivariable optimization with desirability function for carbon porosity and methylene blue adsorption by watermelon rind activated carbon prepared by microwave assisted H3PO4, *Biomass Convers. Biorefin.*, 2022, 1–15.
71 S. Roy, A. K. Saha, S. Panda and G. Dey, Optimization of turmeric oil extraction in an annular supercritical fluid extractor by comparing BBD-RSM and FCCD-RSM approaches, *Mater. Today: Proc.*, 2023, **76**, 47–55.
72 T. Musabeygi, N. Goudarzi, M. Mirzaee and M. Arab-Chamjangali, Design of a ternary magnetic composite based on a covalent organic framework and Ag nanoparticles for simultaneous photodegradation of organic pollutants under LED light irradiation: Application of BBD-RSM modeling and resolution of spectral overlap of analytes, *J. Alloys Compd.*, 2023, **964**, 171249.
73 A. Guesmi, N. B. Hamadi, W. A. El-Fattah, M. A. El-Bindary, M. G. El-Desouky and A. A. El-Bindary, Sustainable cobalt (II) removal from wastewater using an electrospun Ag-MOF/polycaprolactone-chitosan nanofiber membrane: Optimization and regeneration performance, *Int. J. Biol. Macromol.*, 2025, **319**, 145673.
74 W. A. El-Fattah, A. Guesmi, N. B. Hamadi, A. Alzahrani, A. A. Alluhaybi and M. G. El-Desouky, Effective of mercury (II) removal from contaminated water using an innovative nanofiber membrane: Kinetics, isotherms, and optimization studies, *Int. J. Biol. Macromol.*, 2025, **311**, 143596.
75 K. Aziz, F. Aziz, R. Mamouni, L. Aziz and N. Saffaj, Engineering of highly Brachychiton populneus shells@ polyaniline bio-sorbent for efficient removal of pesticides from wastewater: Optimization using BBD-RSM approach, *J. Mol. Liq.*, 2022, **346**, 117092.
76 N. B. Hamadi, A. Guesmi, W. A. El-Fattah, B. H. Alshammari, N. A. Aldawsari, M. G. El-Desouky and A. A. El-Bindary, Design and optimization of chitosan–polyethylenimine encapsulated aluminum–palladium layered double hydroxide for efficient paraquat herbicide adsorption via Box–Behnken approach, *J. Mol. Liq.*, 2025, **437**, 128604.
77 N. B. Hamadi, A. Guesmi, W. A. El-Fattah, M. A. El-Bindary, M. G. El-Desouky and A. A. El-Bindary, Box–Behnken optimization of stimuli-responsive DOX@Ag-MOF/chitosan — Polycaprolactone nanofiber membranes for smart controlled drug delivery and multifunctional therapeutic applications, *Int. J. Biol. Macromol.*, 2025, **330**, 147989.

78 N. A. H. Alshammari, N. H. Elsayed, A. S. Alhawiti, R. A. S. Alatawi, A. A. H. Bukhari, J. S. Alnawmasi, K. B. Alomari, K. M. Alnahdi, H. A. Al-Aoh, M. A. Al-Duais and M. G. El-Desouky, Sustainable nanofibrous cellulose-based hydrogel beads derived from cigarette filter waste, functionalized with hyaluronic acid and encapsulated in chitosan/polyethylenimine for enhanced nickel(II) adsorption from aqueous media, *Int. J. Biol. Macromol.*, 2025, **322**, 146780.

79 A. Latif, A. Maqbool, R. Zhou, M. Arsalan, K. Sun and Y. Si, Optimized degradation of bisphenol A by immobilized laccase from Trametes versicolor using Box-Behnken design (BBD) and artificial neural network (ANN), *J. Environ. Chem. Eng.*, 2022, **10**, 107331.

80 A. Guesmi, N. B. Hamadi, W. A. El-Fattah, A. Subaihi, A. A. Alluhaybi, M. G. El-Desouky and A. A. El-Bindary, Efficient removal of Pb(II) ions from wastewater via a vanadium metal-organic framework encapsulated with biopolymer carboxymethyl cellulose/polyethylenimine through synthesis, characterization, and Box-Behnken optimization, *Int. J. Biol. Macromol.*, 2025, **318**, 145201.

81 W. A. El-Fattah, A. Guesmi, N. B. Hamadi, M. G. El-Desouky and A. A. El-Bindary, Smart nanocomposite of carbon quantum dots in double hydrogel (carboxymethyl cellulose/chitosan) for effectively adsorb and remove diquat herbicide: Characterization, thermodynamics, isotherms, kinetics, and optimizing through Box-Behnken Design, *Int. J. Biol. Macromol.*, 2025, **309**, 142806.

82 H. S. AlSalem, R. A. S. Alatawi, A. A. H. Bukhari, J. S. Alnawmasi, I. Zghab, M. G. El-Desouky, M. H. Almabadi, Z. H. Alnakhli and N. H. Elsayed, Adsorption and removal of Pb (II) via layer double hydroxide encapsulated with chitosan; synthesis, characterization adsorption isotherms, kinetics, thermodynamics, & optimization via Box-Behnken design, *Int. J. Biol. Macromol.*, 2024, **283**, 137517.

83 Z. Wardighi, A. E. Amri, L. Kadiri, A. Jebli, F. Z. Bouhassane and A. Lebkiri, Ecological study of elimination of the organic pollutant (violet crystal) using natural fibers of Rubia tinctorum: Optimization of adsorption processes by BBD-RSM modeling and DFT approaches, *Inorg. Chem. Commun.*, 2023, **155**, 111014.

84 K. Aziz, R. Mamouni, A. Azrrar, B. Kjidaa, N. Saffaj and F. Aziz, Enhanced biosorption of bisphenol A from wastewater using hydroxyapatite elaborated from fish scales and camel bone meal: A RSM@ BBD optimization approach, *Ceram. Int.*, 2022, **48**, 15811–15823.

85 N. B. Hamadi, A. Guesmi, W. Abd El-Fattah, M. A. El-Bindary, M. G. El-Desouky and A. A. El-Bindary, Eco-engineered electrospun La/Rb-MOF/chitosan–PCL nanofibrous membrane for high-performance, recyclable, and sustainable Cr (vi) removal from water, *RSC Adv.*, 2025, **15**, 44766–44796.

86 R. Nazerifard, M. Mohammadpourfard and S. Z. Heris, Optimization of the integrated ORC and carbon capture units coupled to the refinery furnace with the RSM-BBD method, *J. CO_2 Util.*, 2022, **66**, 102289.

87 R. Venkatraman and S. Raghuraman, Experimental analysis on density, micro-hardness, surface roughness and processing time of Acrylonitrile Butadiene Styrene (ABS) through Fused Deposition Modeling (FDM) using Box Behnken Design (BBD), *Mater. Today Commun.*, 2021, **27**, 102353.

88 A. Afzalinia, M. Mirzaee and M. A. Amani, Design of an S-scheme photo-catalyst utilizing a Cu-doped perovskite and MOF-5 for simultaneous degradation of organic pollutants under LED light irradiation: Application of EXRSM method for spectra separation and BBD-RSM modeling, *Spectrochim. Acta, Part A*, 2023, **287**, 122116.

89 Y.-J. Hao, K.-X. Zhang, M.-Y. Jin, X.-C. Piao, M.-L. Lian and J. Jiang, Improving fed-batch culture efficiency of Rhodiola sachalinensis cells and optimizing flash extraction process of polysaccharides from the cultured cells by BBD–RSM, *Ind. Crops Prod.*, 2023, **196**, 116513.

90 N. I. Madondo and M. Chetty, Anaerobic co-digestion of sewage sludge and bio-based glycerol: Optimisation of process variables using one-factor-at-a-time (OFAT) and Box-Behnken Design (BBD) techniques, *S. Afr. J. Chem. Eng.*, 2022, **40**, 87–99.